

RESEARCH PAPER



## Discovery of new 3-methylquinoxalines as potential anti-cancer agents and apoptosis inducers targeting VEGFR-2: design, synthesis, and *in silico* studies

Mohammed M. Alanazi<sup>a</sup> , Elwan Alaa<sup>b</sup> , Nawaf A. Alsaif<sup>a</sup> , Ahmad J. Obaidullah<sup>a</sup> , Hamad M. Alkahtani<sup>a</sup> , Abdulrahman A. Al-Mehizia<sup>a</sup> , Sultan M. Alsubaie<sup>a</sup>, Mohammed S. Taghour<sup>b</sup>  and Ibrahim H. Eissa<sup>b</sup> 

<sup>a</sup>Department of Pharmaceutical Chemistry, College of Pharmacy, King Saud University, Riyadh, Saudi Arabia; <sup>b</sup>Pharmaceutical Medicinal Chemistry and Drug Design Department, Faculty of Pharmacy (Boys), Al-Azhar University, Cairo, Egypt

### ABSTRACT

There is an urgent need to design new anticancer agents that can prevent cancer cell proliferation even with minimal side effects. Accordingly, two new series of 3-methylquinoxalin-2(1H)-one and 3-methylquinoxaline-2-thiol derivatives were designed to act as VEGFR-2 inhibitors. The designed derivatives were synthesised and evaluated *in vitro* as cytotoxic agents against two human cancer cell lines namely, HepG-2 and MCF-7. Also, the synthesised derivatives were assessed for their VEGFR-2 inhibitory effect. The most promising member **11e** were further investigated to reach a valuable insight about its apoptotic effect through cell cycle and apoptosis analyses. Moreover, deep investigations were carried out for compound **11e** using western-blot analyses to detect its effect against some apoptotic and apoptotic parameters including caspase-9, caspase-3, BAX, and Bcl-2. Many *in silico* investigations including docking, ADMET, toxicity studies were performed to predict binding affinity, pharmacokinetic, drug likeness, and toxicity of the synthesised compounds. The results revealed that compounds **11e**, **11g**, **12e**, **12g**, and **12k** exhibited promising cytotoxic activities (IC<sub>50</sub> range is 2.1–9.8 μM), comparing to sorafenib (IC<sub>50</sub> = 3.4 and 2.2 μM against MCF-7 and HepG2, respectively). Moreover, **11b**, **11f**, **11g**, **12e**, **12f**, **12g**, and **12k** showed the highest VEGFR-2 inhibitory activities (IC<sub>50</sub> range is 2.9–5.4 μM), comparing to sorafenib (IC<sub>50</sub> = 3.07 nM). Additionally, compound **11e** had good potential to arrest the HepG2 cell growth at G2/M phase and to induce apoptosis by 49.14% compared to the control cells (9.71%). As well, such compound showed a significant increase in the level of caspase-3 (2.34-fold), caspase-9 (2.34-fold), and BAX (3.14-fold), and a significant decrease in Bcl-2 level (3.13-fold). For *in silico* studies, the synthesised compounds showed binding mode similar to that of the reference compound (sorafenib).

### ARTICLE HISTORY

Received 18 February 2021  
Revised 2 June 2021  
Accepted 14 June 2021

### KEYWORDS

Anticancer; apoptosis; *in silico* studies; 3-methylquinoxalin-2(1H)-one; 3-methylquinoxaline-2-thiol; VEGFR-2 inhibitors



## 1. Introduction


Cancer has been the most difficult and life-threatening illness to be treated<sup>1</sup>. After cardiovascular disease (CVD) cancer has been reported to be a significant cause of death worldwide<sup>2</sup>. At the end of 2018, cancer caused 9.6 million deaths<sup>3</sup>. The current anti-cancer therapy has many side effects arising from non-selectivity of the development of drug resistance<sup>4</sup>. Nonetheless, there is an urgent need to design new anticancer drugs that can prevent cancer cell proliferation even with minimal to no side effects on healthy cells.

At the level of molecular biology, protein tyrosine kinases have an important role in cell proliferation, migration, survival, and progression<sup>5</sup>. Tyrosine kinases phosphorylate the protein's tyrosine residues resulting in altered protein function. In some cases, tyrosine kinases become continuously active which ultimately leads to cancer<sup>6</sup>. Tyrosine kinase receptors (RTKs) are a panel of cell surface receptors that transfer the signal to polypeptides, hormones, and growth factors<sup>7</sup>. There have been numerous known RTKs such as Vascular endothelial growth factor receptors (VEGFRs) and endothelial growth factor receptors (EGFRs)<sup>8</sup>.

VEGFRs have been recognised as an outstanding medicinal target to discover new anticancer agents<sup>9,10</sup>. The class of VEGFRs comprises three subtypes; VEGFR-1, VEGFR-2, and VEGFR-3<sup>11</sup>. Among them, VEGFR-2 which has a crucial role in tumour angiogenesis. VEGFR-2 can be activated through binding with VEGF which starts the process of phosphorylation which boosts proliferation and migration of the endothelial cells<sup>12</sup>. VEGFR-2 is mainly overexpressed throughout endothelial cells of the tumour vasculature, with less expression in normal endothelial cells<sup>13</sup>. Hepatocellular carcinoma and breast cancer are well-known examples of tumours with overexpressed VEGFR-2<sup>14–16</sup>.

VEGFR-2 inhibitors are small molecules that bind at the ATP binding site of VEGFR-2 to inhibit angiogenesis and lymphangiogenesis<sup>17</sup>. Beside many VEGFR-2 inhibitors approved by FDA or under clinical trials, there are a lot of effort to discover new ones for the management of cancer. Sorafenib **I** is a bi-aryl urea, has inhibitory effect against tyrosine kinases involved in tumour development, including VEGFR-2<sup>18</sup>. Sunitinib **II** is anti-tumour drug with dual activity against VEGFR-2 and PDGFR-β<sup>19</sup>. Telatinib **III** is an orally active anti-VEGFR-2 small-molecule<sup>20</sup>. Nintedanib **IV** is a potent small-molecule tyrosine kinase inhibitor with oral activity.

**CONTACT** Ibrahim H. Eissa  [Ibrahimeissa@azhar.edu.eg](mailto:Ibrahimeissa@azhar.edu.eg)  Pharmaceutical Medicinal Chemistry and Drug Design Department, Faculty of Pharmacy (Boys), Al-Azhar University, Cairo, 11884, Egypt

 Supplemental data for this article can be accessed [here](#).

© 2021 The Author(s). Published by Informa UK Limited, trading as Taylor & Francis Group.

This is an Open Access article distributed under the terms of the Creative Commons Attribution License (<http://creativecommons.org/licenses/by/4.0/>), which permits unrestricted use, distribution, and reproduction in any medium, provided the original work is properly cited.

In addition, it has a triple angiokinase inhibitory effect as it inhibits the three major signalling pathways involved in angiogenesis<sup>21</sup>. Acrizanib **V** is a VEGFR-2 inhibitor with limited systemic exposure after topical ocular administration<sup>22</sup>. Vorolanib **VI** is a novel indolinone-based kinase inhibitor that targets the VEGFR-2<sup>23</sup>. It has fewer adverse effects and a wide therapeutic window<sup>24</sup>.

Essential Pharmacophoric features of VEGFR-2 inhibitors have been reported in many publications<sup>25–30</sup>. The reported pharmacophore includes: i) a flat hetero aromatic moiety which binds Cys917 via a hydrogen bonding interaction<sup>26</sup>, (ii) a spacer moiety which occupies the area between the ATP-binding domain and the DFG domain<sup>31</sup>, (iii) a pharmacophore moiety which consists of H-bond acceptor (HBA) and one H-bond donor (HBD) groups (e.g. amide or urea). Both HBA and HBD have a key binding role, as they form hydrogen bonding interactions with two crucial residues (Glu883 and Asp1044)<sup>32</sup>, and (iv) a terminal hydrophobic moiety can make many hydrophobic interactions in the allosteric hydrophobic pocket of VEGFR-2<sup>33</sup> (Figures 1 and 2).

In the current work, ligand-based drug design approach<sup>34–37</sup> was used to synthesise two series of 3-methylquinoxalin-2(1*H*)-one and 3-methylquinoxaline-2-thiol derivatives. This work is an extension of the earlier activities of our team to synthesise effective anticancer agents targeting VEGFR-2<sup>9,38,39</sup>. The synthesised derivatives were evaluated *in vitro* and *in silico* to assess their VEGFR-2 inhibitory activities.

### 1.1. Rationale of molecular design

VEGFR-2 inhibitors competitively block the ATP binding site which consists of four main regions. i) Hinge region which is occupied by the flat hetero aromatic ring of VEGFR-2 inhibitors. ii) Gatekeeper region which is occupied by the spacer moiety of VEGFR-2 inhibitors. iii) DFG-motif region which is occupied by the pharmacophore moiety of VEGFR-2 inhibitors. iv) Allosteric hydrophobic region which is occupied by the terminal hydrophobic moiety of VEGFR-2 inhibitors<sup>33,40–42</sup> (Figure 2).

The main objective of our design was the synthesis of new compounds having the main pharmacophoric features of VEGFR-2 inhibitors. Such compounds comprise different bio-isosteres, each of them occupy a specific region at ATP binding site.

For the hinge region, two quinoxaline moieties were used; i) 3-methylquinoxalin-2(1*H*)-one (compounds **11a–j**) and ii) 3-methylquinoxaline-2-thiol (compounds **12a–k**). The bicyclic structure of quinoxaline moiety is suitable to the large size space of the ATP binding region<sup>43</sup>. In addition, the nitrogen atoms act as hydrogen-bond acceptors to facilitate the hydrogen bonding interaction with the hinge region. The Gatekeeper region was targeted to be occupied by *N*-phenylacetamide moiety as spacer group. Regarding the DFG-motif region, an amide group (pharmacophore moiety) was selected to be buried in it. Finally, the allosteric hydrophobic region can be occupied by different aliphatic and aromatic derivatives to study the structure-activity relationships (Figure 2).

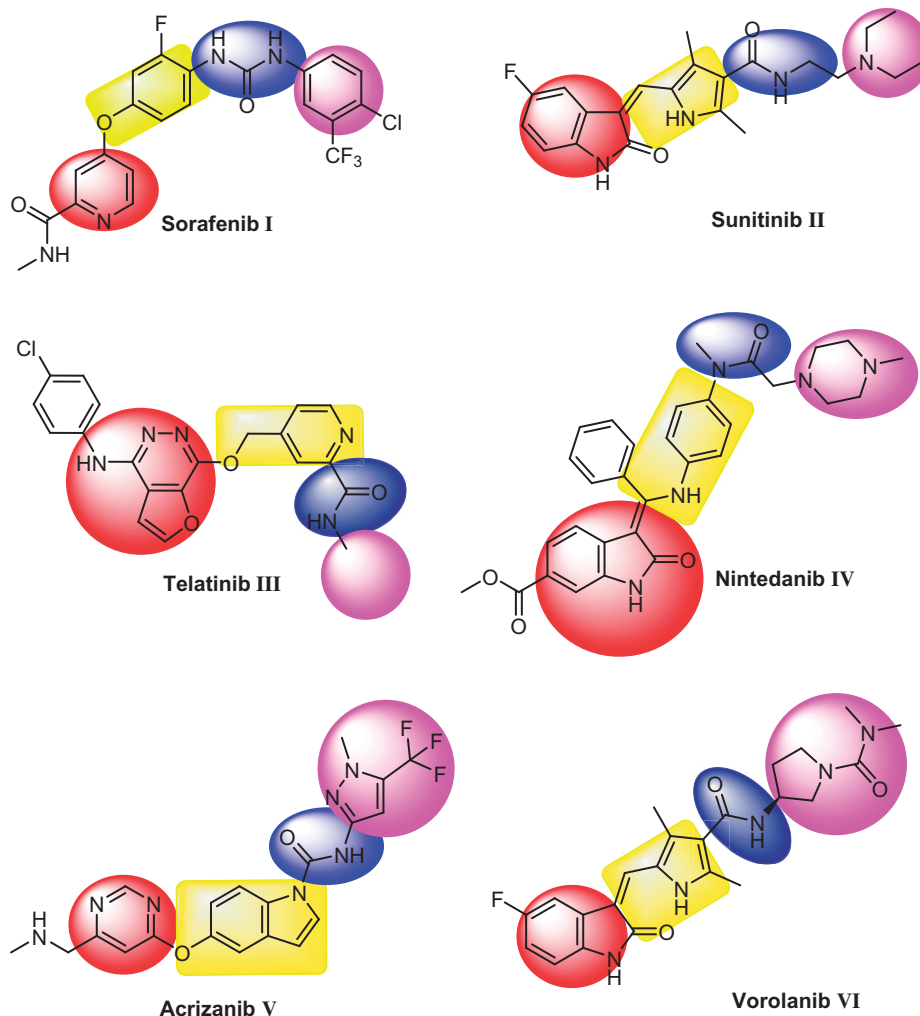
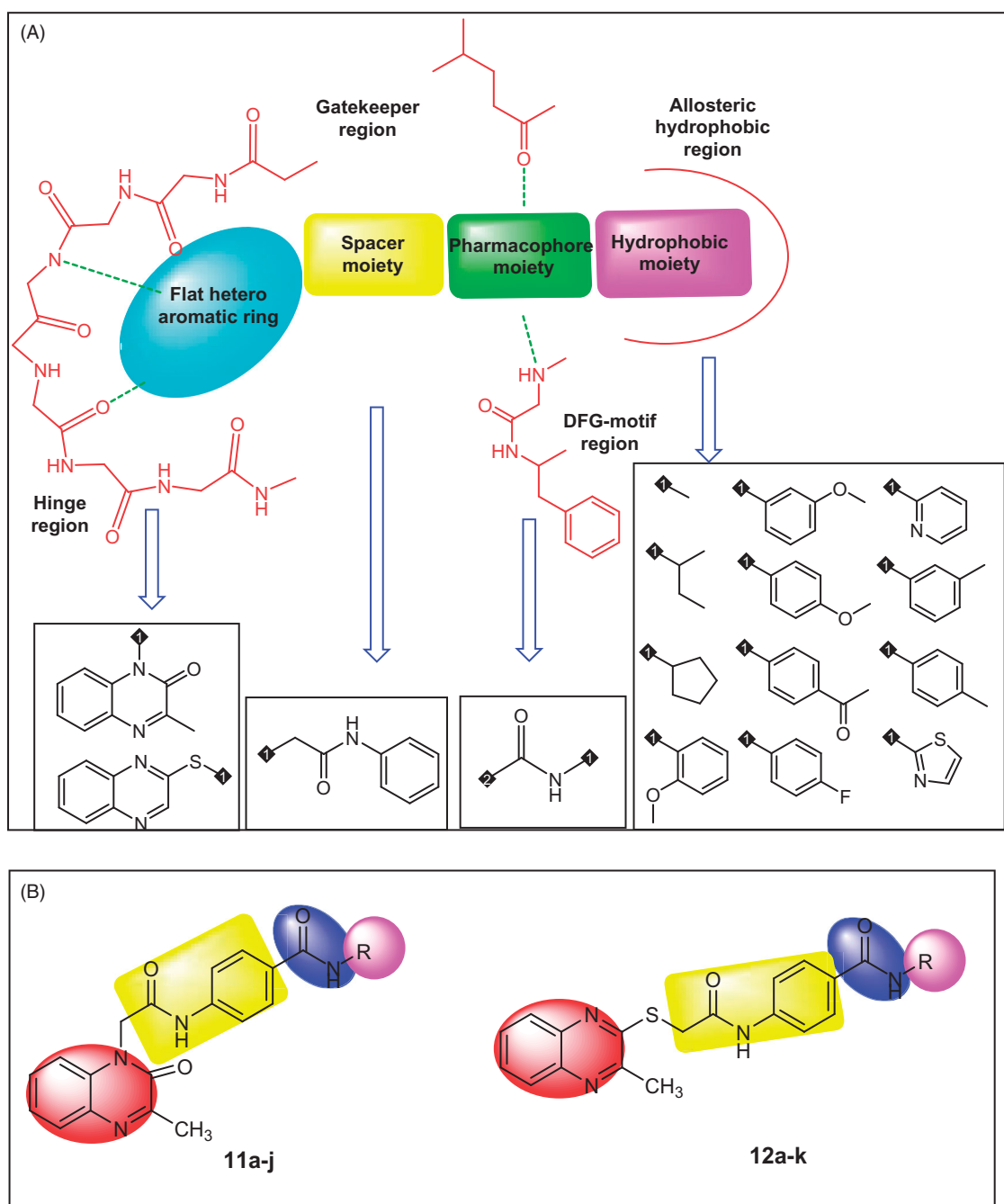


Figure 1. Some reported VEGFR-2 inhibitors and their basic pharmacophoric features.



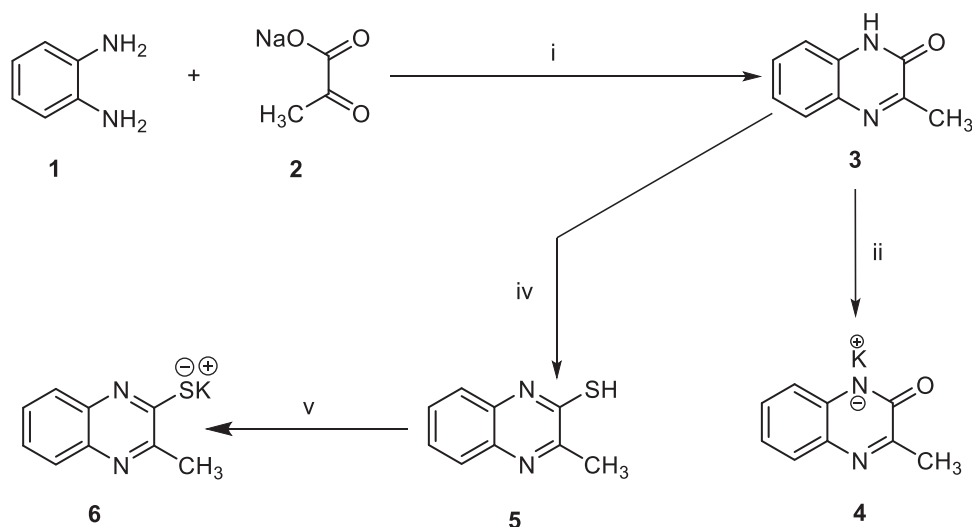
**Figure 2.** A) Different bio-isosteres that can occupy the ATP binding site of VEGFR-2. B) Representative examples of the new synthesised compounds having the same essential pharmacophoric features of VEGFR-2 inhibitor.

## 2. Results and discussion

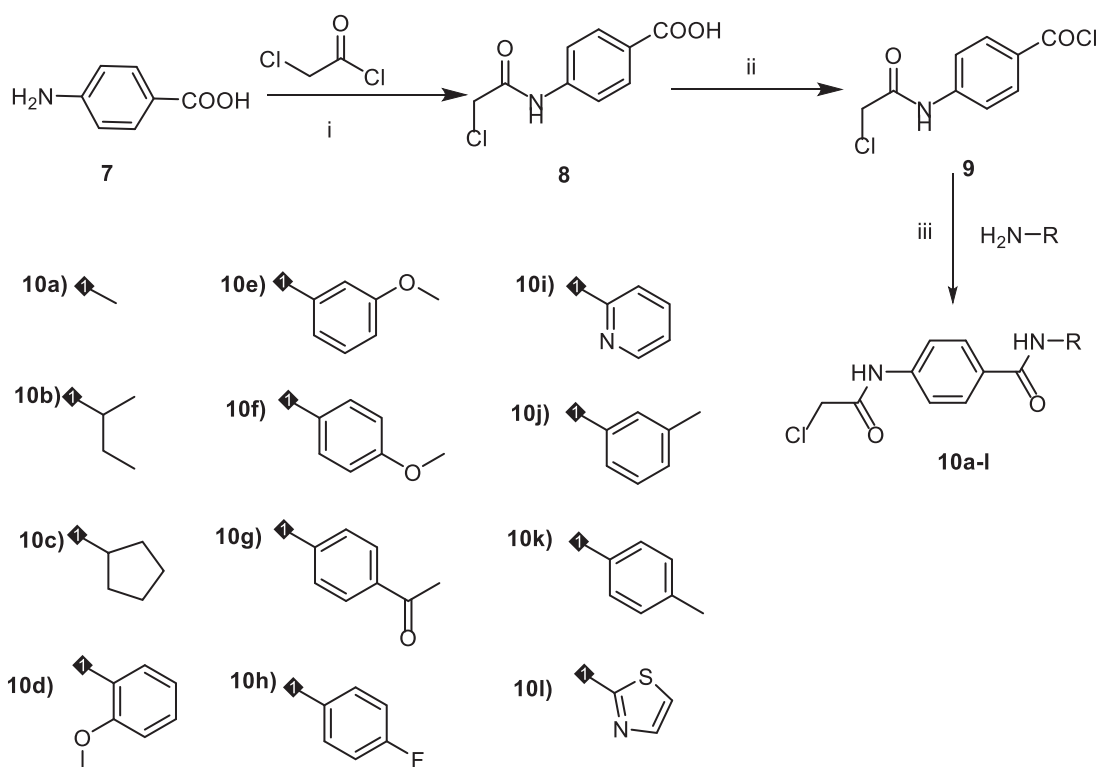
### 2.1. Chemistry

In order to synthesise the designed compounds, Schemes 1–4 were adopted. Initially, *o*-phenylenediamine **1** was refluxed with sodium pyruvate **2** to afford 3-methylquinoxalin-2(1*H*)-one **3** according to the reported procedure<sup>44</sup>. Subsequent heating of compound **3** with alcoholic potassium hydroxide gave the corresponding potassium salt **4**<sup>44</sup>. To prepare 3-methylquinoxaline-2-thiol **5**, the previously prepared 3-methylquinoxalin-2(1*H*)-one **3** was refluxed with P<sub>2</sub>S<sub>5</sub> in pyridine as a solvent, then the reaction was acidified using HCl<sup>45,46</sup>. Heating of compound **5** with alcoholic potassium hydroxide gave the corresponding potassium salt **6** (Scheme 1).

The key intermediates were synthesised as described in Scheme 2. The commercially available *p*-amino benzoic acid **7** was treated with chloroacetyl chloride in dry DMF in the presence of NaHCO<sub>3</sub> to afford 4-(2-chloroacetamido)benzoic acid **8**. Chlorination of **8** was achieved by its reflux with SOCl<sub>2</sub> in dichloroethane in the presence of catalytic amount of dry DMF to give the key compound 4-(2-chloroacetamido)benzoyl chloride **9**. At the end, in acetonitrile and TEA mixture, compound **9** was stirred at room temperature with appropriate amines namely, methylamine, *sec*-butylamine, cyclopentylamine, 2-methoxyaniline, 3-methoxyaniline, 4-methoxyaniline, 4-aminoacetophenone, 4-fluoroaniline, 2-aminopyridine, *m*-toluidine, *p*-toluidine, and 2-aminothiazole to give the corresponding key intermediates **10a–l**, respectively. The IR spectra of the key intermediates **10a–l**



**Scheme 1.** synthesis of compound key potassium salts **4** and **5**. **Reagents and conditions:** i) g. acetic acid/H<sub>2</sub>O/reflux/2 h, ii) Alc. KOH/reflux/30 min., iii) i) P<sub>2</sub>S<sub>5</sub>/pyridine/reflux/2 h then HCl, v) Alc. KOH/reflux/30 min.



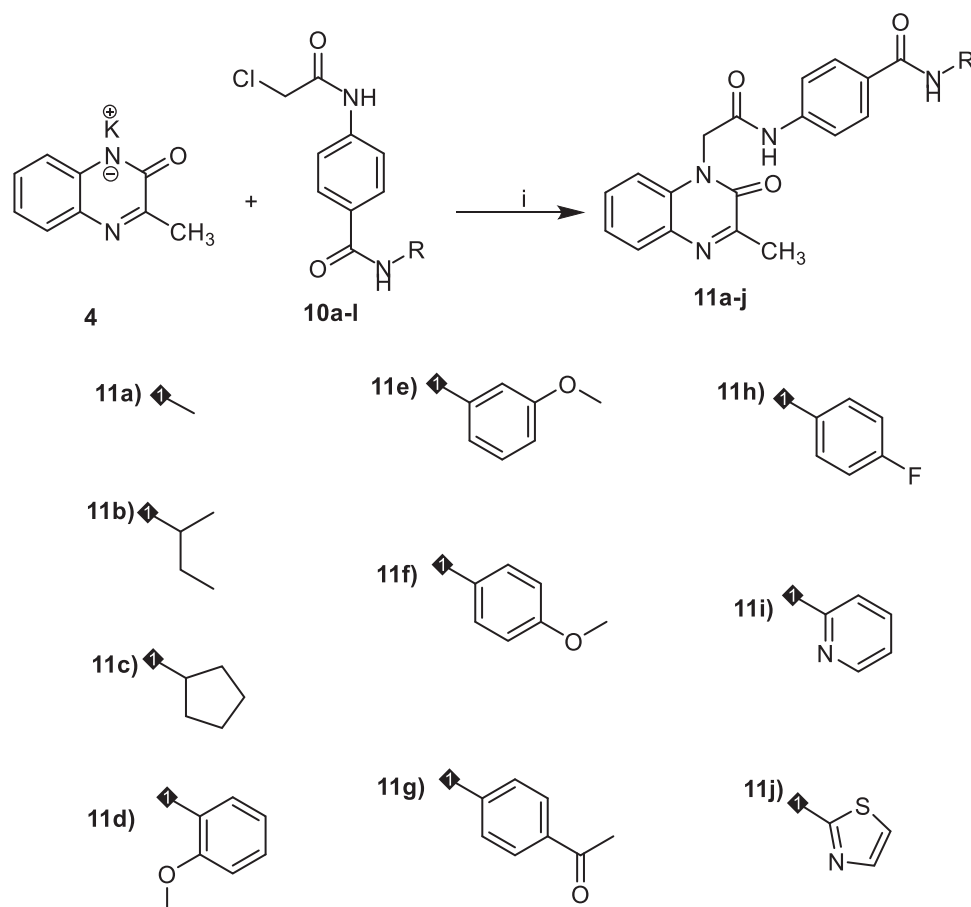
**Scheme 2.** synthesis of the key intermediates **10a-l**. **Reagents and conditions:** i) DMF/NaHCO<sub>3</sub>/stirring, r.t./1h, ii) dichloroethane/SOCl<sub>2</sub>/DMF/reflux/1h, iii) CH<sub>3</sub>CN/stirring/r.t./3h.

exhibited the appearance of absorption bands at the ranges of 3254–3326 cm<sup>-1</sup> and 1702–1625 cm<sup>-1</sup> due to the NH and 2C=O groups, respectively. In addition, <sup>1</sup>H NMR analyses exhibited the appearance of characteristic singlet signals for amidic NHs around  $\delta$  10.00 ppm. Also, it showed singlet signals for CH<sub>2</sub> protons of acetamide moiety around  $\delta$  4.30 ppm. Besides, such CH<sub>2</sub> group was detected around  $\delta$  44.02 ppm in <sup>13</sup>C NMR spectra.

The first series of the target compounds was prepared as described in Scheme 3. The potassium salt of 3-methylquinoxalin-2(1H)-one **4** was heated in dry DMF with the keys intermediates in the presence of catalytic amount of KI to give the titled compounds **11a-j**.

The second series of the target compounds was synthesised depending on the synthetic pathway described in Scheme 4. The potassium salt of methylquinoxaline-2-thiol **6** was heated in dry DMF with the keys intermediates **10a-k** in the presence of catalytic amount of KI to give the titled compounds **12a-k**.

<sup>1</sup>H NMR spectra exhibited the presence of singlet signals of CH<sub>3</sub> group of 3-methylquinoxalin-2(1H)-one moiety around  $\delta$  2.49 ppm. In addition, <sup>1</sup>H NMR spectra showed characteristic signals for additional aromatic and aliphatic protons at the expected chemical shift. Taken compound **11c** and **12c** as representative examples, it showed many characteristic signals at aliphatic region corresponding to cyclopentyl moiety. Moreover, <sup>13</sup>C NMR spectra



**Scheme 3.** synthesis of the target compounds 11a-j. **Reagents and conditions:** i) KI/DMF/heating/W.B./8h.

of such compounds confirmed the previous results as the aliphatic protons of cyclopentyl moiety appeared at the aliphatic region.

## 2.2. Biological testing

### 2.2.1. In vitro cytotoxic activities

Cytotoxic activities of the synthesised compounds were evaluated against MCF-7 (human breast cancer cell line) and HepG2 (human liver carcinoma cell line) using MTT assay<sup>47</sup>, using sorafenib as a reference standard (Table 1). Among the target compounds, **11e**, **11g**, **12e**, **12g**, and **12k** exhibited promising cytotoxicity against the two cell lines with  $IC_{50}$  values ranging from 2.1 to 9.8  $\mu$ M, comparing to sorafenib ( $IC_{50}$  = 3.4 and 2.2  $\mu$ M against MCF-7 and HepG2, respectively). Compound **11e** exhibited a superior activity against MCF-7 and HepG2 with  $IC_{50}$  values of 2.7 and 2.1, respectively. In addition, compounds **11f** and **12f** showed promising activity against HepG2 cells with  $IC_{50}$  values of 9.6 and 7.5, respectively. Compounds **11a**, **11b**, **11c**, **12c**, and **12d** showed moderate activity against HepG2 cells with  $IC_{50}$  values of 16.5, 12.8, 18.7, 11.4, 18.7, and 17.6  $\mu$ M, respectively. In addition, compounds **11f** and **12f** showed moderate activity against MCF-7 cells with  $IC_{50}$  values of 12.4 and 10.8  $\mu$ M, respectively. On the other hand, compounds **11d**, **11h**, **11i**, **11j**, **12a**, and **12b** showed weak cytotoxic activity against the two cell lines.

### 2.2.2. Vegfr-2 inhibitory assay

VEGFR-2 inhibitory activity of the synthesised compounds was investigated using sorafenib as a reference drug. Table 1.

Summarised the  $IC_{50}$  values of VEGFR-2 growth inhibitory concentration for all the synthesised members.

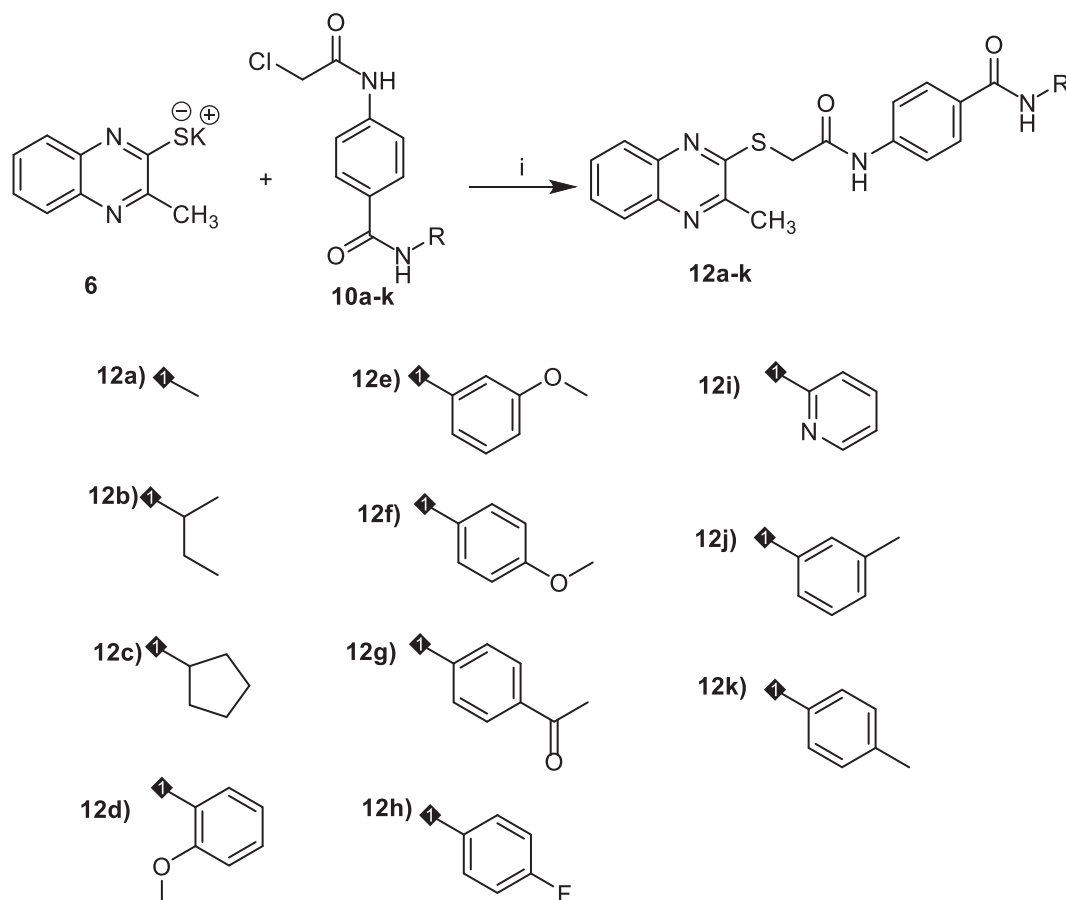
Compound **11e** and **12k** exhibited VEGFR-2 inhibitory activity ( $IC_{50}$  = 2.6 and 2.9 nM, respectively) higher than that of sorafenib ( $IC_{50}$  = 3.07 nM). Additionally, compounds **11b**, **11f**, **11g**, **12e**, **12f**, **12g**, and **12k** showed promising activities with  $IC_{50}$  values ranging from 2.9 to 5.4 nM. On the other hand, compounds **11a**, **11c**, **11d**, **11h**, **11i**, **11j**, **12a**, **12b**, **12c**, **12d**, **12h**, **12i**, and **12j** showed moderate to weak activity. Its  $IC_{50}$  values are ranging from 11.2 to 52.7 nM.

### 2.2.3. Statistical correlation between VEGFR-2 inhibition and cytotoxicity

To study the relation between cytotoxicity and VEGFR-2 inhibition, we plotted the values of VEGFR-2 inhibition against the corresponding cytotoxicity results using simple linear regression analysis. Co-efficient of determination ( $R^2$ ) were calculated in this analysis. It was found that  $R^2$  of VEGFR-2 inhibition and MCF-7 cytotoxicity is 0.887 with  $p$  values  $>0.0001$ . In addition,  $R^2$  of VEGFR-2 inhibition and HepG2 cytotoxicity is 0.887 with  $p$  values  $>0.0001$ . The results indicated that there are high correlations between VEGFR-2 inhibition and cytotoxic activity on both cell lines, which reveals that the cytotoxicity may be a result of VEGFR-2 inhibition (Figure 3).

### 2.2.4. Structure-Activity relationship (SAR)

The results of different biological analyses (cytotoxic activity and VEGFR-2 inhibitory assay) gave a valuable SAR. Initially, the effect



**Scheme 4.** synthesis of the target compounds **12a-k**. Reagents and conditions: i) KI/DMF/heating/W.B./8h.

**Table 1.** *In vitro* cytotoxic and VEGFR-2inhibitory activities.

Comp.	Cytotoxicity IC <sub>50</sub> ( μM ) <sup>a</sup>		VEGFR-2 inhibitory activity IC <sub>50</sub> ( nM ) <sup>a</sup>
	MCF-7	HepG2	
11a	23.9	16.5	11.2
11b	21.2	12.8	5.3
11c	28.1	18.7	12.7
11d	52.3	34.1	37.4
11e	2.7	2.1	2.6
11f	12.4	9.6	4.8
11g	6.7	3.8	3.4
11h	25.8	22.7	11.6
11i	69.7	51.8	52.7
11j	32.8	27.8	13.4
12a	69.2	23.7	32.7
12b	35.7	21.7	15.7
12c	31.3	18.7	19.8
12d	23.5	17.6	13.4
12e	5.3	4.8	3.8
12f	10.8	7.5	3.8
12g	8.7	6.1	5.4
12h	67.8	35.8	51.4
12i	58.6	44.7	24.1
12j	61.2	40.7	37.8
12k	9.8	6.7	2.9
Sorafenib	3.4	2.2	3.1

<sup>a</sup>All IC<sub>50</sub> values are calculated as the mean of at least three different experiments.

of the flat hetero aromatic ring on the activity was explored. Comparing the cytotoxic activity of compounds **11a-j** (incorporating 3-methylquinoxalin-2(1*H*)-one) with compounds **12a-k** (incorporating 3-methylquinoxaline-2-thiol) indicated that

3-methylquinoxalin-2(1*H*)-one moiety is more advantageous than 3-methylquinoxaline-2-thiol moiety for cytotoxic and VEGFR-2 inhibitory effects.

Then, we investigated the effect of the terminal hydrophobic moiety. Comparing the activity of compounds **11a-c** and **12a-c** having aliphatic hydrophobic moieties with compounds **11e-g** and **12e-g** having aromatic hydrophobic moieties indicated that aromatic moieties are beneficial for activity. For aliphatic moieties, there is no great variation in the activity among small size (compound **11a** and **12a**), bulk (compound **11c** and **12c**), and branched (compound **11b** and **12b**) aliphatic moieties.

In addition, the effect of the substitution on the aromatic hydrophobic moieties has been investigated. Comparing the activity of compound **12k** (incorporating 4-methylphenyl moiety) and compounds **11f** and **12f** (incorporating 4-methoxyphenyl moiety) with compounds **11h** and **12h** (incorporating 4-fluorophenyl) and compounds **11g** and **12g** (incorporating acetophenone moiety), revealed that grafting an electron donating group is more preferred biologically than electron withdrawing one. For electron withdrawing groups, it was found that acetyl incorporating members (**11g** and **12g**) are more active than fluoro incorporating one (**11h** and **12h**).

Next, the effect of the substitution on the aromatic hydrophobic moieties with electron donating group has been examined. For methylquinoxalin-2(1*H*)-one derivatives, the activities reduced in the order of 3-methoxy (**11e**) > 4-methoxy (**11f**) > 2-methoxy (**11d**). With regard to 3-methylquinoxaline-2-thiol derivatives, the activities decreased in the order of 4-methyl (**12k**) > 3-methoxy (**12e**) > 4-methoxy (**12f**) > 2-methoxy (**12d**) > 3-methoxy (**12j**).

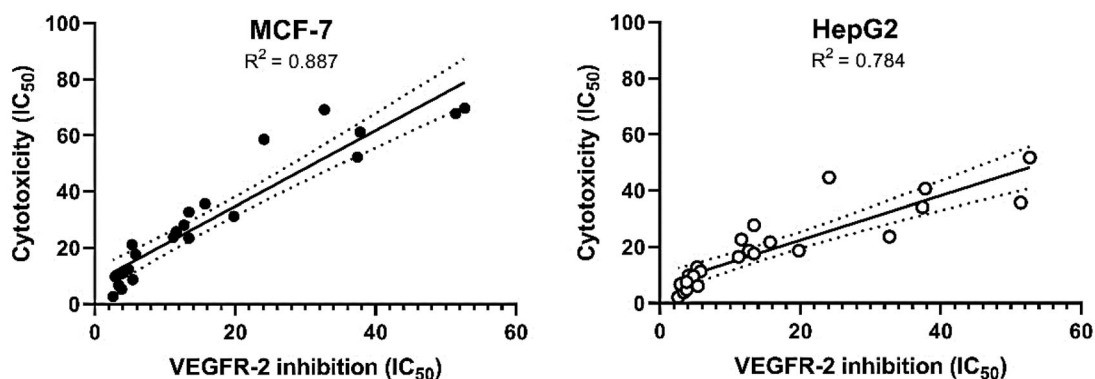


Figure 3. Simple linear regression for the correlation between VEGFR-2 inhibition and cytotoxicity.

Table 2. *In vitro* cytotoxicity of the most active compounds (**11e** and **12e**) and sorafenib against normal cells (primary rat hepatocytes).

Comp.	IC <sub>50</sub> (μM) <sup>a</sup> primary rat hepatocytes
<b>11e</b>	15.0
<b>12e</b>	16.7
Sorafenib	13.4

<sup>a</sup>IC<sub>50</sub> values are the mean of three separate experiments.

Finally, the decreased IC<sub>50</sub> values of compound **11j** (with thiazole moiety) against the tested cell lines and VEGFR-2 than the IC<sub>50</sub> values of compound **11i** (with pyridine moiety), indicated that five-membered hetero aromatic hydrophobic moiety is more efficient than six-membered one.

### 2.2.5. *In vitro* cytotoxicity against normal cell

The cytotoxicities of the most active compounds (**11e** and **12e**) against primary rat hepatocytes (normal hepatic cells) were evaluated *in vitro* (Table 2). The results revealed that the tested compounds have low toxicity against the tested cells with IC<sub>50</sub> values of 15.0 and 16.7 μM, respectively. Sorafenib as a reference drug showed IC<sub>50</sub> value of 13.4 μM against the tested cells. These results revealed that the synthesised compounds have low toxicity against the normal cells as their toxicities are comparable to that of FDA approved drug (sorafenib).

### 2.2.6. Cell cycle analysis

The cell cycle is a well-maintained process by which cells of eukaryotes replicate themselves. The homeostatic balance between cell loss and cell gain must be achieved to produce and conserve the complex architecture of tissues. One way in which this connection may be achieved is through the coupling of the cell cycle and apoptosis<sup>48</sup>.

Since compound **11e** effectively inhibited the growth of HepG2 cells, it was expected that this inhibitory effect was due to its capability to hinder the cell cycle progression. Therefore, cell cycle process was analysed after exposure of HepG2 cells to **11e** with a concentration of 2.1 μM (IC<sub>50</sub> value of compound **11e**) after 24 h. HepG2 cells were used as a control without treatment by compound **11e**. Flow cytometry data revealed that the percentage of cells arrested at the G2/M phase increased from 18.24% (in control cells) to 46.62 (in **11e** treated cells). In addition, the percentage of HepG2 cells mild increased at the S phase from 25.48 to 31.80%. Oppositely, the percentage of HepG2 cells decreased at G1 phase from 55.03% to 20.34%. Such findings revealed that

compound **11e** arrested the HepG2 cell growth at G2/M phase (Figure 4 and Supplementary Data).

### 2.2.7. Apoptosis analysis

To quantify the apoptosis triggered by **11e**, Annexin-V/propidium iodide (PI) staining assay was conducted. In such procedure, compound **11e** at a concentration of 2.1 μM was applied on HepG2 cells. Then, the media were incubated for 24 h. As shown in Table 3, the apoptotic effect of **11e** in HepG2 cells was five times more than observed in control cells. In details, compound **11e** induced apoptosis by 49.14% (early apoptosis = 48.87% & late apoptosis = 0.27%), compared to 9.71% in the control cells (early apoptosis = 9.58% & late apoptosis = 0.13%).

### 2.2.8. Western blot analysis

Apoptosis is a programmed cell death characterised by some biological processes including condensation of nuclear chromatin, loss of plasma membrane phospholipid asymmetry, DNA cleavage into small fragments, and formation of membrane-bound apoptotic bodies<sup>49</sup>.

During intrinsic apoptosis, caspase-9 is activated to produce a subsequent activation of other effector caspases. It was reported that caspase-9 is a highly specific protease that only cleaves a few proteins, whereas caspase-3 contributes to the majority of cleavage that takes place during apoptosis<sup>50,51</sup>. Additionally, the mitochondrial apoptosis is largely mediated through Bcl-2 family proteins, which include. i) Pro-apoptotic members such as BAX that promote mitochondrial permeability and cell death. ii) Anti-apoptotic members such as Bcl-2 that inhibit the mitochondrial release of cyt c and suppress cell death<sup>52</sup>. According to these reports, a cell with a high BAX/Bcl-2 ratio will be more sensitive to some given apoptotic stimuli when compared to a similar cell type with a low BAX/Bcl-2 ratio<sup>53</sup>.

**2.2.8.1. Caspase-3 and caspase-9 determination.** To investigate the effect of the synthesised compounds on caspase-3 and caspase-9 levels, the most promising member **11e** was applied on the most sensitive cells (HepG2) at a concentration of 2.1 μM for 24 h. Western blot analyses revealed that compound **11e** produced a significant increase in the level of caspase-3 (2.34-fold) compared to the control cells. Moreover, compound **11e** showed a significant increase in the level of caspase-9 (2.34-fold) compared to the control cells (Figure 5 and Supplementary Data).

**2.2.8.2. BAX and Bcl-2 determination.** Compound **11e** as a promising member was investigated to evaluate its effect on BAX and

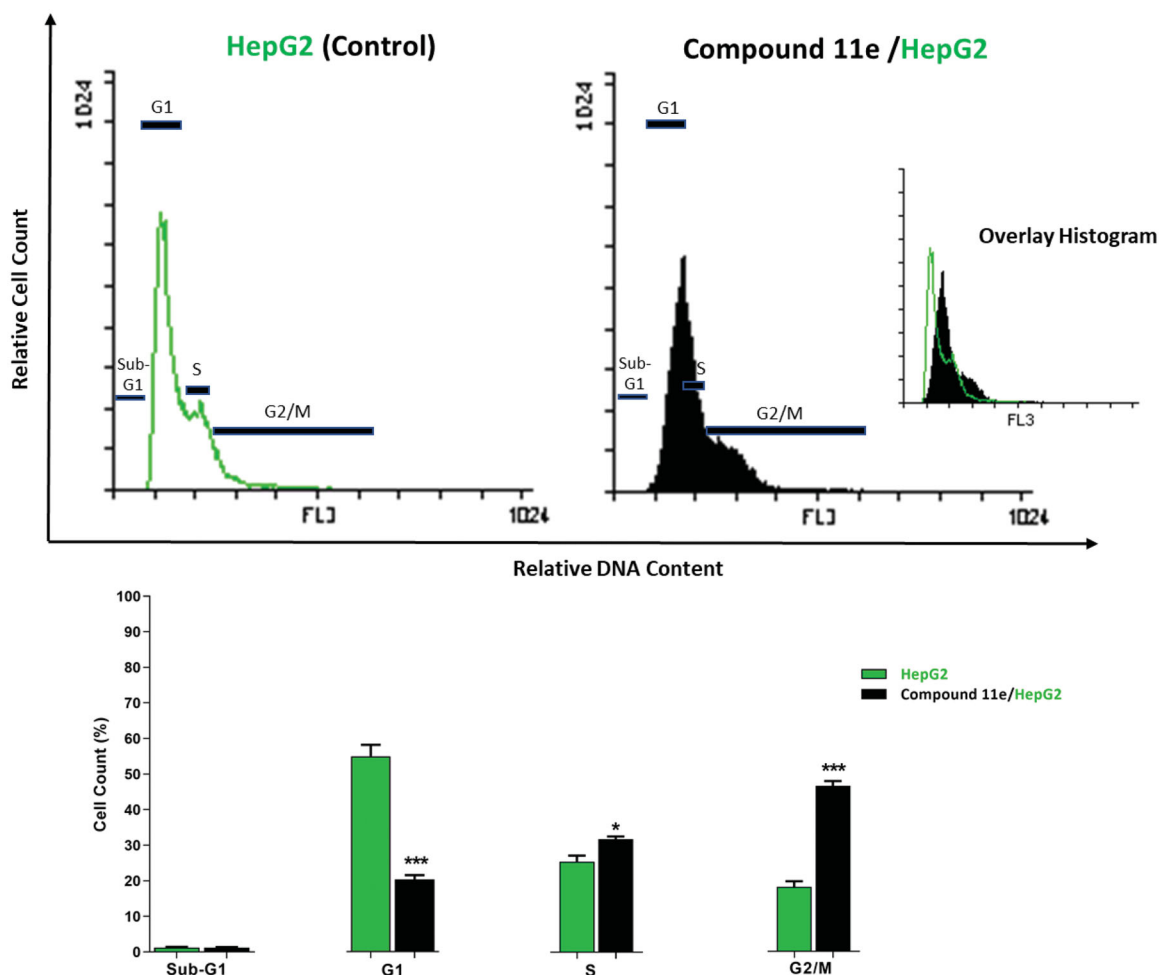


Figure 4. Flow cytometric analysis of cell cycle phases post the compound 11e treatment.

Table 3. Effect of compound 11e on stages of the cell death process in HepG2 cells after 24 h treatment.

Sample	Viable <sup>a</sup> (Left Bottom)	Apoptosis <sup>a</sup>		Necrosis <sup>a</sup> (Left Top)
		Early (Right Bottom)	Late (Right Top)	
HepG2	90.20 ± 1.07	9.58 ± 0.86	0.13 ± 0.01	0.10 ± 0.02
Compound 11e /HepG2	50.65 ± 3.66	48.87 ± 3.69	0.27 ± 0.04	0.20 ± 0.03

<sup>a</sup>Values are reported as mean ± SD of three different experiments.

Bcl-2 after 24 h of its application on HepG2 cells using Western blot technique. The results showed that compound 11e produced an up-regulation of BAX and down-regulation of Bcl-2. In details, BAX level increased by 3.14-fold, while Bcl-2 level decreased by 3.13-fold. In addition, BAX/Bcl-2 ratio was 9.17, which indicated that compound 11e had a significant effect on apoptosis pathway (Figure 5 and Supplementary Data).

### 2.3. In silico studies

#### 2.3.1. Docking studies

In this work, the synthesised compounds were docked against VEGFR-2 using sorafenib as a reference drug. This investigational work was performed to get further insight into the binding modes of the synthesised compounds against VEGFR-2 binding site (PDB ID: 2OH4). The binding free energies ( $\Delta G$ ) for all the synthesised compounds against the target receptor were calculated and reported in Table 4. The reported key binding site of VEGFR-2

consists of Glu883 and Asp1044<sup>33,54</sup>. Validation of the docking procedure and the binding mode of the reference drug (sorafenib)<sup>33,54</sup> were showed in Supplementary data.

The synthesised compounds exhibited binding mode inside the binding sites of VEGFR-2 similar to that of sorafenib. Compound 11e was completely buried inside VEGFR-2 active site with similar binding mode to sorafenib. The docking score of such compound was  $-28.81$  kcal/mol. The pharmacophore moiety (amide group) was incorporated in hydrogen bonding interaction forming a hydrogen bond with Glu883 and another one with Asp1044. The phenyl group (spacer) formed three hydrophobic interactions with Val914 and Cys1043. The 3-methylquinoxalin-2(1H)-one nucleus was inserted in hinge region of the binding pocket forming five hydrophobic interactions with Leu1033, Phe916, Ala864, and Leu838. In addition, the terminal methoxyphenyl group (hydrophobic tail) formed one hydrophobic bond with Leu887. Additionally, it formed two electrostatic interactions with Asp1044 (Figure 6).

Regarding compound 11a (incorporating methyl group as hydrophobic tail) showed binding energy of  $-22.37$  kcal/mol. It showed binding mode similar to that of sorafenib with some deviations. Firstly, due to lack of bulk aromatic moiety (as appeared in compound 11e), this led to disappearance of hydrophobic interactions at the allosteric binding pocket of VEGFR-2. In addition, the orientation of 3-methylquinoxalin-2(1H)-one nucleus at the hinge region prevent the hydrogen bonding interaction with Cys917 (Figure 7).

With respect to compound 12a, it exhibited a binding mode like that of sorafenib with binding energy of  $-27.98$  kcal/mol. The



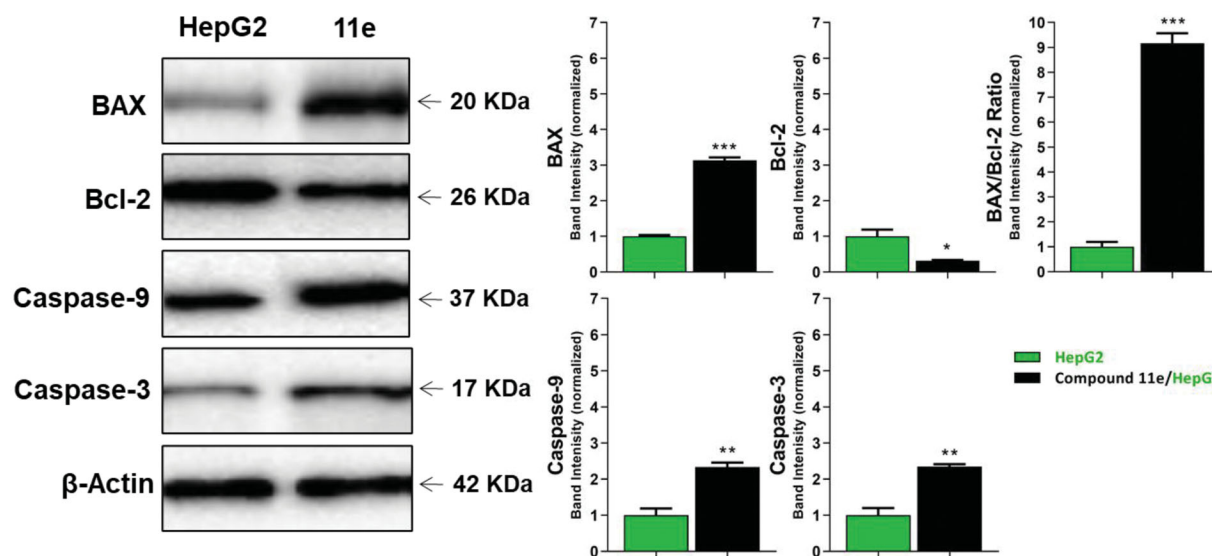


**Figure 5.** The immunoblotting of BAX, Bcl-2, Caspase-9, and Caspase-3 (Normalized to  $\beta$ -actin).

**Table 4.** Binding free energies ( $\Delta G$  in Kcal/mol) of the synthesised compounds and sorafenib against VEGFR-2

Comp. No.	$\Delta G$ [Kcal/mol]	Compound	$\Delta G$ [Kcal/mol]
11a	-22.37	12b	-27.03
11b	-28.35	12c	-28.20
11c	-28.03	12d	-28.95
11d	-27.90	12e	-27.98
11e	-28.81	12f	-29.16
11f	-28.79	12g	-30.11
11g	-30.62	12h	-28.26
11h	-27.26	12i	-27.58
11i	-27.00	12j	-29.46
11j	-25.38	12k	-28.73
12a	-21.81	Sorafenib	-25.69

different features of compounds **12a** occupied the same regions which occupied by sorafenib. However, elongation of the linker moiety exerted mild change in the orientation of 3-methylquinoxaline-2-thiol nucleus at the hinge region preventing the hydrogen bonding interaction with Cys917 (Figure 8).

### 2.3.2. In silico ADMET studies

The *in silico* ADMET parameters were assessed via Discovery studio 4.0 using Sorafenib as a reference molecule.

The results revealed that the tested compounds have low or very low BBB penetration levels except for compounds **12h**, **12j**, and **12k** which were predicted to have medium levels. Accordingly, most compounds were anticipated to be safe against CNS. Furthermore, compounds **11a-g**, **11i**, and **11j** were predicted to have good levels of aqueous solubility, while compounds **12a-k** were predicted to have low levels. Moreover, intestinal absorption levels of all the tested compounds were predicted to be good. The cytochrome P4502D6 inhibition was predicted using CYP2D6 model<sup>55</sup>. All the tested compounds were predicted as non-inhibitors of CYP2D6. So that, these compounds are expected to be safe for the liver. The plasma protein binding (PPB) model predicts the degree of molecule binding to PP. If it is  $\geq 90\%$ , it means that a molecule can bind the PP at high concentration<sup>56</sup>. Compounds **11c-e**, **11g-i**, **12h**, **12i**, and **12k** were expected to bind plasma protein over 90%, while compounds **11a**, **11b**, **11f**, **11j**, **12a-g**, and **12i** were predicted to bind plasma protein less than 90% (Table 5, Figure 9).

### 2.3.3. In silico toxicity studies

Discovery studio 4.0 was used to determine the expected toxicity potential of the synthesised compounds<sup>57,58</sup>.

As shown in Table 6, most compounds showed *in silico* low toxicity profile against the tested models. Compounds **11a-j** and **12a,b** were predicted to have carcinogenic potency  $TD_{50}$  values ranging from 19.427 to 81.588 mg/kg body weight/day, which were higher than that of sorafenib (carcinogenic potency  $TD_{50}$  = 19.236 mg/kg body weight/day). While compounds **12c-k** were estimated to have low carcinogenic potency  $TD_{50}$  values (from 7.026 to 17.638 mg/kg body weight/day). In addition, the rat maximum tolerated doses of compounds **11h**, **12b**, and **12h-k** were estimated to be between 0.133 and 0.096 g/kg body weight, which were higher than that of sorafenib (rat maximum tolerated dose = 0.089 g/kg body weight). The other derivatives were predicted to have fewer rat maximum tolerated doses. Moreover, compounds **11a-c**, **11g**, **11i**, **11j**, **12a**, **12c**, **12g**, **12i**, and **12k** were predicted to be non-toxic against developmental toxicity potential model. For rat oral  $LD_{50}$  model, the tested compounds showed oral  $LD_{50}$  values ranging from 2.102 to 18.807 g/kg body weight/day. Such values are far more than that of sorafenib (oral  $LD_{50}$  = 0.823 g/kg body weight/day). Moreover, all the tested compounds were predicted to be mild irritant against ocular irritancy model, and non-irritant against skin irritancy model.

## 3. Conclusion

Twenty-two compounds were designed, synthesised, and evaluated as VEGFR-2 inhibitors. Such derivatives were assessed against MCF-7 and HepG-2 cell lines to estimate its antiproliferative activities. Compounds **11e**, **11g**, **12e**, **12g**, and **12k** displayed promising cytotoxic activities against MCF-7 and HepG-2 with  $IC_{50}$  values ranging from 2.1 to 9.8  $\mu M$ . Furthermore, compounds **11b**, **11e**, **11f**, **11g**, **12e**, **12f**, **12g**, and **12k** showed VEGFR-2 inhibitory activities with  $IC_{50}$  values of 5.3, 2.6, 4.8, 3.4, 3.8, 3.8, 5.4, and 2.9 nM, respectively. SAR revealed that 3-methylquinoxalin-2(1H)-one moiety is more beneficial than 3-methylquinoxaline-2-thiol moiety for cytotoxicity and VEGFR-2 inhibitory activities. Also, the terminal aromatic moieties were found to be more valuable than the terminal aliphatic ones. Compound **11e**, the most potent member, arrested the HepG2 cell growth at G2/M phase and induced apoptosis by 49.14% compared to the control cells

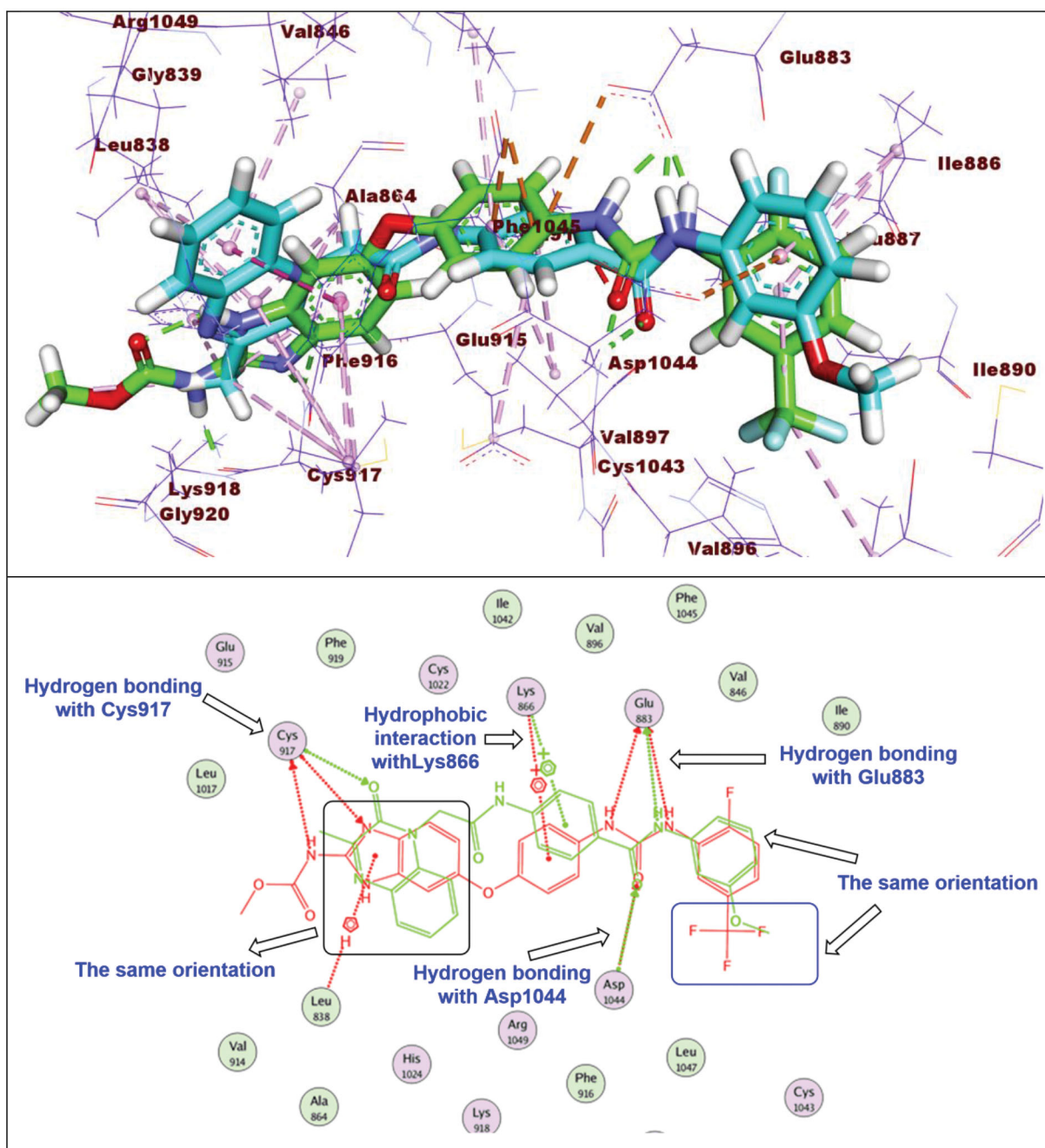


**Figure 6.** Superimposition of compound **11e** and sorafenib inside the active sites of VEGFR-2. Compound **11e** was completely buried inside VEGFR-2 active site with similar binding mode to sorafenib.

(9.71%). Additionally, such derivative showed a significant elevation in the level of caspase-3 (2.34-fold) and caspase-9 (2.34-fold). Moreover, it showed a marked increase in BAX (3.14-fold) and a significant reduction in Bcl-2 level (3.13-fold). The *in silico* studies revealed that the synthesised compounds showed binding interactions like that of sorafenib with good drug likeness profile.

## 4. Experimental

### 4.1. Chemistry

#### 4.1.1. General

Reagents, solvent, and apparatus used in chemical synthesis were showed in [Supplementary data](#). Compounds **3**, **4**, **5**, **6**, **8**, **9**, **10a-l** were prepared according to reported procedures<sup>44–46,59–64</sup>.

Physical, elemental, and spectral data of the intermediate compounds **10a-l** were depicted in [Supplementary data](#).

#### General procedure for synthesis of compounds **11a-j**

To a solution of the potassium salt of 3-methylquinoxalin-2(1H)-one **4** (320 mg, 0.002 mol) in DMF (20 ml) the appropriate 4-(2-chloroacetamido)-*N*-substituted-benzamides **10a-i** and **10l** (0.002 mol) was added. The mixture was heated on a water bath for 10 h. After cooling to room temperature, the reaction mixture was poured onto crushed ice. The precipitated solids were filtered, dried and crystallised from ethanol to give the target compounds **11a-j**.

**4.1.1.1. N-Methyl-4-(2-(3-methyl-2-oxoquinoxalin-1(2H)-yl)acetamido)benzamide 11a.** White powder (yield 75%); mp: 294–297 °C; FT-IR (ν max, cm<sup>-1</sup>): 3288 (NH), 1674, 1655 (C=O), 1601 (C=N); <sup>1</sup>H NMR (700 MHz, DMSO-*d*<sub>6</sub>) δ 10.68 (s, 1H), 8.34 (q, *J*=4.6 Hz, 1H),

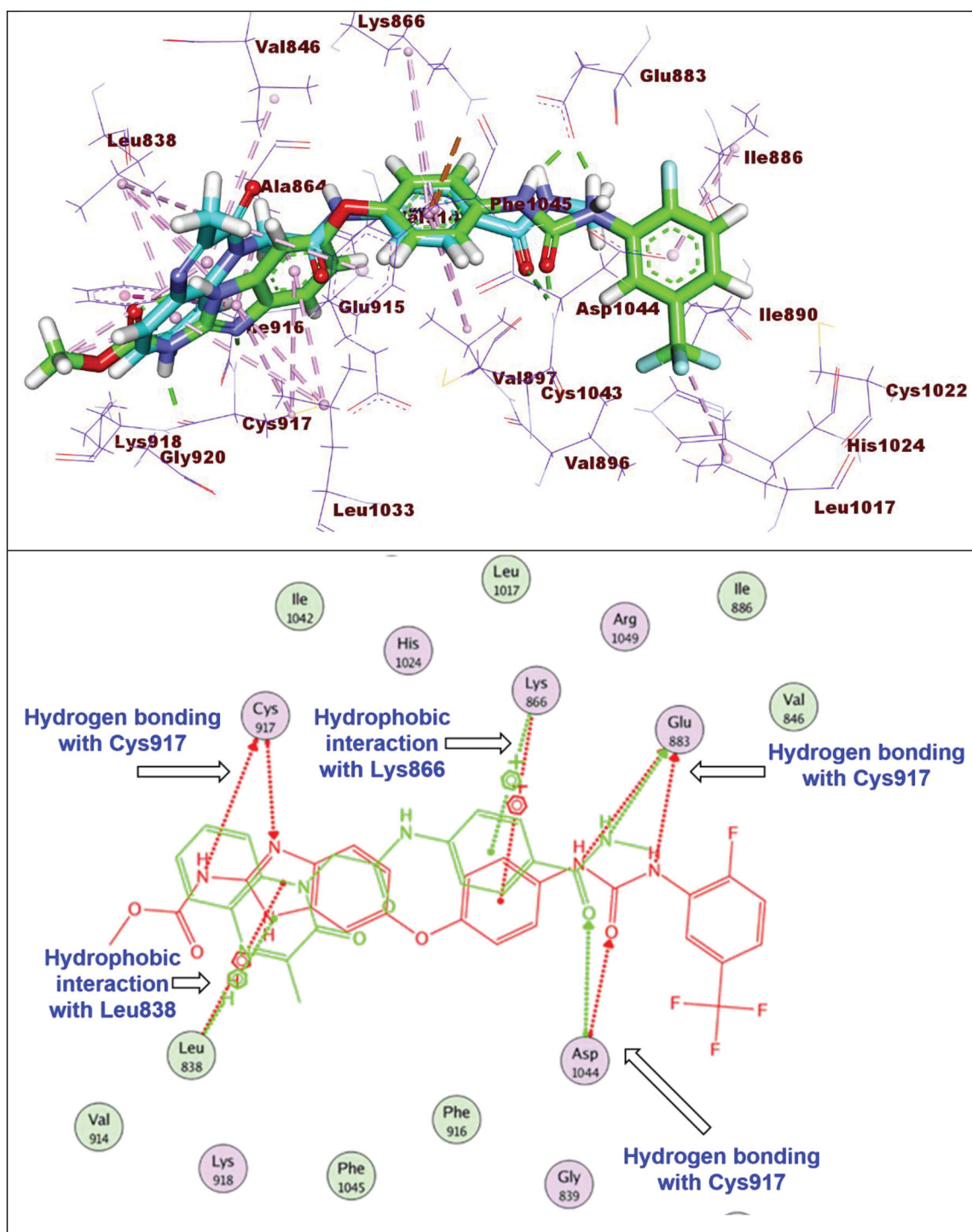


**Figure 7.** Superimposition of compound **11a** and sorafenib inside the active sites of VEGFR-2. Compound **11a** showed binding mode similar to that of sorafenib with lack of hydrophobic interaction inside the allosteric binding pocket and absence of hydrogen bonding interaction with Cys917 at hinge region.

7.83–7.79 (m, 3H), 7.64 (d,  $J=8.8$  Hz, 2H), 7.57 (t,  $J=8.5$  Hz, 1H), 7.52 (d,  $J=8.4$  Hz, 1H), 7.38 (t,  $J=7.5$  Hz, 1H), 5.16 (s, 2H), 2.76 (s, 3H), 2.49 (s, 3H);  $^{13}\text{C}$  NMR (176 MHz, DMSO)  $\delta$  166.46, 165.68, 157.97, 154.84, 141.46, 133.46, 132.46, 130.18, 129.87, 129.27, 128.47 (2C), 123.92, 118.81 (2C), 115.19, 45.75, 26.66, 21.59; MS ( $m/z$ ): 351 ( $M^+ + 1$ , 15% %), 201 (60%); Anal. Calcd. for  $\text{C}_{19}\text{H}_{18}\text{N}_4\text{O}_3$  (350.38): C, 65.13; H, 5.18; N, 15.99; Found: C, 65.53; H, 5.06; N, 15.64%.

**4.1.1.2. *N*-(*sec*-Butyl)-4-(2-(3-methyl-2-oxoquinoxalin-1(2H)-yl)acetamido)benzamide **11b**.** White powder (yield 70%); mp:

319–321 °C; FT-IR ( $\nu$  max,  $\text{cm}^{-1}$ ): 3275 (NH), 2965 (CH aliphatic), 1660, 1634 (C=O), 1600 (C=N);  $^1\text{H}$  NMR (700 MHz, DMSO- $d_6$ )  $\delta$  10.68 (s, 1H), 8.04 (d,  $J=8.2$  Hz, 1H), 7.85–7.82 (m, 2H), 7.81 (dd,  $J=8.0$ , 1.5 Hz, 1H), 7.66–7.62 (m, 2H), 7.57 (ddd,  $J=8.6$ , 7.1, 1.5 Hz, 1H), 7.53 (dd,  $J=8.5$ , 1.3 Hz, 1H), 7.38 (ddd,  $J=8.2$ , 7.1, 1.3 Hz, 1H), 5.16 (s, 2H), 3.91 (ddd,  $J=14.1$ , 7.6, 6.2 Hz, 1H), 2.49 (s, 3H), 1.58–1.44 (m, 2H), 1.13 (d,  $J=6.6$  Hz, 3H), 0.86 (t,  $J=7.4$  Hz, 3H);  $^{13}\text{C}$  NMR (176 MHz, DMSO- $d_6$ )  $\delta$  165.66, 165.44, 157.96, 154.85, 141.39, 133.47, 132.46, 130.22, 130.18, 129.27, 128.65 (2C), 123.92, 118.69 (2C), 115.20, 46.81, 45.75, 29.32, 21.59, 20.77, 11.25;

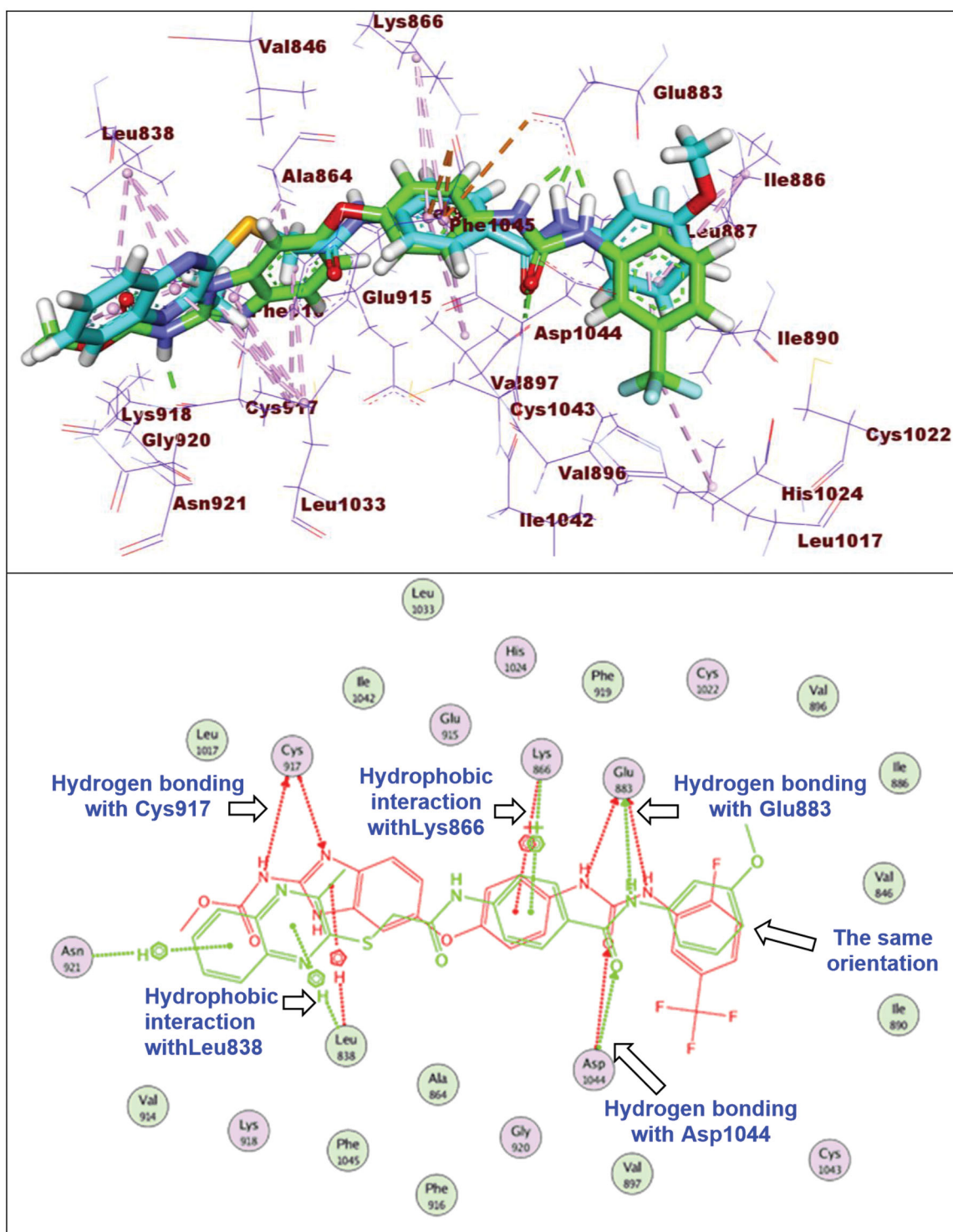


**Figure 8.** Superimposition of compound 12e and sorafenib inside the active sites of VEGFR-2. Compound 12e showed binding mode similar to that of sorafenib with lack of hydrogen bonding interaction with Cys917 at hinge region.

MS ( $m/z$ ): 393 ( $M^+ + 1$ , 80%); Anal. Calcd. for  $C_{22}H_{24}N_4O_3$  (392.46): C, 67.33; H, 6.16; N, 14.28; Found: C, 66.94; H, 6.34; N, 13.95%.

**4.1.1.3. *N*-Cyclopentyl-4-(2-(3-methyl-2-oxoquinoxalin-1(2H)-yl)acetamido)benzamide 11c.** Brown powder (yield 72%); mp: 298 – 300 °C; FT-IR ( $\nu$  max,  $cm^{-1}$ ): 3281 (NH), 2953 (CH aliphatic), 1631 (C=O), 1603 (C=N);  $^1H$  NMR (700 MHz, DMSO- $d_6$ )  $\delta$  10.69 (s,

1H), 8.18 (d,  $J=7.6$  Hz, 1H), 7.84 (d,  $J=8.2$  Hz, 2H), 7.80 (d,  $J=8.0$  Hz, 1H), 7.64 (d,  $J=8.4$  Hz, 2H), 7.57 (t,  $J=7.7$  Hz, 1H), 7.53 (d,  $J=8.4$  Hz, 1H), 7.37 (t,  $J=7.5$  Hz, 1H), 5.16 (s, 2H), 4.22 (h,  $J=6.6$  Hz, 1H), 2.49 (s, 3H), 1.91 – 1.84 (m, 2H), 1.69 (m, 2H), 1.53 (m,  $J=7.4$  Hz, 4H);  $^{13}C$  NMR (176 MHz, DMSO- $d_6$ )  $\delta$  165.70, 165.66, 157.95, 154.84, 141.41, 133.46, 132.46, 130.17, 130.09, 129.27 (2C), 128.72, 123.90, 118.66 (2C), 115.18, 51.35, 45.75, 32.61 (2C), 24.09

**Table 5.** Calculated ADMET descriptors

Comp.	BBB level <sup>a</sup>	Solubility level <sup>b</sup>	Absorption level <sup>c</sup>	CYP2D6 prediction <sup>d</sup>	PPB prediction <sup>e</sup>
11a	3	3	0	X	X
11b	3	3	0	X	X
11c	3	3	0	X	√
11d	3	3	0	X	√
11e	3	3	0	X	√
11f	3	3	0	X	X
11g	4	3	0	X	√
11h	3	2	0	X	√
11i	3	3	0	X	√
11j	3	3	0	X	X
12a	3	2	0	X	X
12b	2	2	0	X	X
12c	2	2	0	X	X
12d	4	2	0	X	X
12e	4	2	0	X	X
12f	4	2	0	X	X
12g	4	2	0	X	X
12h	2	2	0	X	√
12i	3	2	0	X	X
12j	2	2	0	X	√
12k	2	2	0	X	√
Sorafenib	4	1	0	X	√

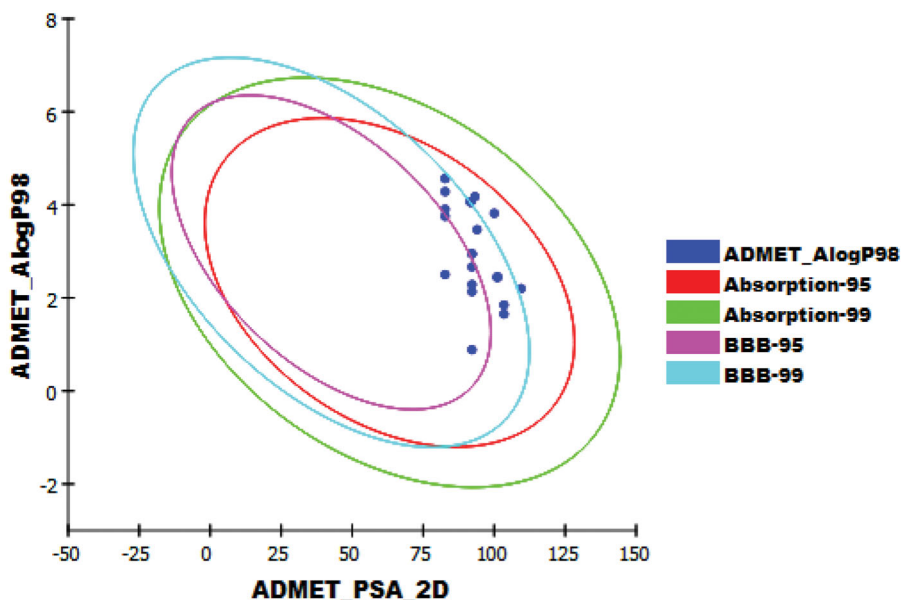
<sup>a</sup>BBB means blood brain barrier which may be very high (0), high (1), medium (2), low (3), or very low (4).

<sup>b</sup>Solubility level may be very low (1), low (2), good (3), or optimal (4).

<sup>c</sup>Absorption level may be good (0), moderate (1), poor (2), or very poor (3).

<sup>d</sup>CYP2D6 means cytochrome P2D6 which may be inhibitor (,) or non-inhibitor (X).

<sup>e</sup>PPB means plasma protein binding which may be less than 90% (X) or more than 90% (,).

**Figure 9.** The expected ADMET study.

(2 C), 21.58; MS ( $m/z$ ): 405 ( $M^+ + 1$ , 50% %), 330 (100%); Anal. Calcd. for  $C_{23}H_{24}N_4O_3$  (404.47): C, 68.30; H, 5.98; N, 13.85; Found: C, 68.65; H, 6.13; N, 13.52%.

**4.1.1.4. *N*-(2-Methoxyphenyl)-4-(2-(3-methyl-2-oxoquinoxalin-1(2H)-yl)acetamido)benzamide 11d.** Grey powder (yield 74%); mp: 265 – 267 °C; FT-IR ( $\nu$  max,  $cm^{-1}$ ): 3289, 3040 (NH), 2922 (CH aliphatic), 1659 (C=O), 1602 (C=N);  $^1H$  NMR (700 MHz, DMSO- $d_6$ )  $\delta$  10.77 (s, 1H), 9.33 (s, 1H), 7.98 – 7.93 (m, 2H), 7.80 (ddd,  $J=19.3$ , 7.9, 1.6 Hz, 2H), 7.75 – 7.70 (m, 2H), 7.58 (ddd,  $J=8.5$ , 7.0, 1.5 Hz, 1H), 7.54 (dd,  $J=8.5$ , 1.3 Hz, 1H), 7.39 (ddd,  $J=8.1$ , 7.0, 1.3 Hz, 1H), 7.18 (td,  $J=7.8$ , 1.7 Hz, 1H), 7.10 (dd,  $J=8.3$ , 1.4 Hz, 1H), 6.97 (td,  $J=7.7$ , 1.4 Hz, 1H), 5.18 (s, 2H), 3.84 (s, 3H), 2.49 (s, 3H);  $^{13}C$  NMR (176 MHz, DMSO- $d_6$ )  $\delta$  165.81, 165.25, 159.87, 157.97, 154.85,

142.03, 140.91, 133.47, 132.47, 130.20, 130.01, 129.82, 129.29, 129.22 (2 C), 123.94, 118.82 (2 C), 115.21, 112.98, 109.49, 106.45, 55.46, 45.80, 21.59; MS ( $m/z$ ): 443 ( $M^+ + 40$ ); Anal. Calcd. for  $C_{25}H_{22}N_4O_4$  (442.48): C, 67.86; H, 5.01; N, 12.66; Found: C, 68.03; H, 4.77; N, 12.36%.

**4.1.1.5. *N*-(3-Methoxyphenyl)-4-(2-(3-methyl-2-oxoquinoxalin-1(2H)-yl)acetamido)benzamide 11e.** Grey powder (yield 70%); mp: 237 – 239 °C; FT-IR ( $\nu$  max,  $cm^{-1}$ ): 3273 (NH), 2922 (CH aliphatic), 1655 (C=O), 1604 (C=N);  $^1H$  NMR (700 MHz, DMSO- $d_6$ )  $\delta$  10.77 (s, 1H), 10.11 (s, 1H), 7.98 – 7.94 (m, 2H), 7.81 (dd,  $J=8.1$ , 1.5 Hz, 1H), 7.72 (d,  $J=8.7$  Hz, 2H), 7.58 (td,  $J=7.7$ , 6.9, 1.5 Hz, 1H), 7.54 (d,  $J=8.4$  Hz, 1H), 7.47 (t,  $J=2.2$  Hz, 1H), 7.41 – 7.35 (m, 2H), 7.25 (t,  $J=8.1$  Hz, 1H), 6.68 (dd,  $J=8.3$ , 2.5 Hz, 1H), 5.18 (s, 2H), 3.76 (s,

**Table 6.** Toxicity properties of the synthesised compounds.

Comp.	Carcinogenic Potency TD <sub>50</sub> (Mouse) <sup>a</sup>	Rat Maximum Tolerated Dose (Feed) <sup>b</sup>	Developmental Toxicity Potential	Rat Oral LD <sub>50</sub> <sup>b</sup>	Ocular Irritancy	Skin Irritancy
11a	81.588	0.056	Non-Toxic	6.255	Mild	Non-Irritant
11b	68.438	0.076	Non-Toxic	15.151	Mild	Non-Irritant
11c	33.606	0.063	Non-Toxic	7.417	Mild	Non-Irritant
11d	48.211	0.043	Toxic	4.609	Mild	Non-Irritant
11e	62.412	0.043	Toxic	9.772	Mild	Non-Irritant
11f	37.877	0.043	Toxic	6.249	Mild	Non-Irritant
11g	51.779	0.060	Non-Toxic	8.214	Mild	Non-Irritant
11h	26.216	0.103	Toxic	6.088	Mild	Non-Irritant
11i	32.099	0.070	Non-Toxic	5.862	Mild	Non-Irritant
11j	40.916	0.048	Non-Toxic	9.349	Mild	Non-Irritant
12a	23.269	0.072	Non-Toxic	6.323	Mild	Non-Irritant
12b	19.427	0.104	Toxic	8.109	Mild	Non-Irritant
12c	9.528	0.080	Non-Toxic	4.965	Mild	Non-Irritant
12d	13.624	0.056	Toxic	2.102	Mild	Non-Irritant
12e	17.638	0.056	Toxic	4.761	Mild	Non-Irritant
12f	10.704	0.056	Toxic	3.045	Mild	Non-Irritant
12g	14.619	0.081	Non-Toxic	4.779	Mild	Non-Irritant
12h	7.416	0.133	Toxic	4.066	Mild	Non-Irritant
12i	9.093	0.100	Non-Toxic	3.499	Mild	Non-Irritant
12j	11.577	0.096	Toxic	11.265	Mild	Non-Irritant
12k	7.026	0.096	Non-Toxic	15.912	Mild	Non-Irritant
Sorafenib	19.236	0.089	Toxic	0.823	Mild	Non-Irritant

<sup>a</sup>Unit: mg/kg body weight/day.<sup>b</sup>Unit: g/kg body weight.

3H), 2.49 (s, 3H); <sup>13</sup>C NMR (176 MHz, DMSO-*d*<sub>6</sub>) δ 165.81, 165.25, 159.87, 157.97, 154.85, 142.03, 140.91, 133.47, 132.47, 130.20, 130.01, 129.82, 129.29, 129.22(2C), 123.94, 118.82 (2C), 115.21, 112.98, 109.49, 106.45, 55.46, 45.80, 21.59; MS (*m/z*): 443 (M<sup>+</sup> + 1, 40% %); Anal. Calcd. for C<sub>25</sub>H<sub>22</sub>N<sub>4</sub>O<sub>4</sub> (442.48): C, 67.86; H, 5.01; N, 12.66; Found: C, 67.50; H, 4.95; N, 12.25%.

**4.1.1.6. N-(4-Methoxyphenyl)-4-(2-(3-methyl-2-oxoquinoxalin-1(2H)-yl)acetamido)benzamide 11f.** Yellow crystals (yield 76%); mp: 324 – 227 °C; FT-IR (ν max, cm<sup>-1</sup>): 3269 (NH), 2957, 2834 (CH aliphatic), 1655 (C=O), 1601 (C=N); <sup>1</sup>H NMR (700 MHz, DMSO-*d*<sub>6</sub>) δ 10.76 (s, 1H), 10.03 (s, 1H), 7.97 – 7.95 (m, 2H), 7.81 (dd, *J* = 8.0, 1.5 Hz, 1H), 7.73 – 7.70 (m, 2H), 7.68 – 7.66 (m, 2H), 7.58 (ddd, *J* = 8.5, 7.0, 1.5 Hz, 1H), 7.54 (dd, *J* = 8.5, 1.3 Hz, 1H), 7.38 (ddd, *J* = 8.1, 7.1, 1.3 Hz, 1H), 6.95 – 6.90 (m, 2H), 5.18 (s, 2H), 3.75 (s, 3H), 2.51 (s, 3H); <sup>13</sup>C NMR (176 MHz, DMSO-*d*<sub>6</sub>) δ 165.77, 164.81, 157.97, 155.92, 154.85, 141.84, 133.47, 132.76, 132.47, 130.19, 130.14, 129.28 (2C), 129.08, 123.94, 122.41(2C), 118.82(2C), 115.20, 114.18(2C), 55.63, 45.79, 21.59; MS (*m/z*): 443 (M<sup>+</sup> + 1, 100%); Anal. Calcd. for C<sub>25</sub>H<sub>22</sub>N<sub>4</sub>O<sub>4</sub> (442.48): C, 67.86; H, 5.01; N, 12.66; Found: C, 67.33; H, 4.97; N, 12.22%.

**4.1.1.7. N-(4-Acetylphenyl)-4-(2-(3-methyl-2-oxoquinoxalin-1(2H)-yl)acetamido)benzamide 11g.** White crystals (yield 71%); mp: 313 – 315 °C; FT-IR (ν max, cm<sup>-1</sup>): 3281 (NH), 2921 (CH aliphatic), 1659 (C=O), 1603 (C=N); <sup>1</sup>H NMR (700 MHz, DMSO-*d*<sub>6</sub>) δ 10.82 (s, 1H), 10.46 (s, 1H), 8.02 – 7.96 (m, 4H), 7.95 (d, *J* = 9.0 Hz, 2H), 7.81 (dd, *J* = 7.9, 1.5 Hz, 1H), 7.79 – 7.73 (m, 2H), 7.58 (ddd, *J* = 8.5, 6.9, 1.5 Hz, 1H), 7.54 (dd, *J* = 8.6, 1.5 Hz, 1H), 7.38 (ddd, *J* = 8.2, 7.0, 1.4 Hz, 1H), 5.19 (s, 2H), 2.55 (s, 3H), 2.49 (s, 3H); <sup>13</sup>C NMR (176 MHz, DMSO-*d*<sub>6</sub>) δ 197.05, 165.87, 165.64, 157.96, 154.85, 144.19, 142.34, 133.46, 132.47, 132.35, 130.19, 129.76 (2C), 129.57, 129.46 (2C), 129.29, 123.93, 119.84(2C), 118.87 (2C), 115.20, 45.81, 26.94, 21.59; Anal. Calcd. for C<sub>26</sub>H<sub>22</sub>N<sub>4</sub>O<sub>4</sub> (454.49): C, 68.71; H, 4.88; N, 12.33; Found: C, 69.03; H, 4.71; N, 11.92%.

**4.1.1.8. N-(4-Fluorophenyl)-4-(2-(3-methyl-2-oxoquinoxalin-1(2H)-yl)acetamido)benzamide 11h.** White powder (yield 72%); mp:

260 – 262 °C; FT-IR (ν max, cm<sup>-1</sup>): 3274 (NH), 3038 (CH aromatic), 2945 (CH aliphatic), 1666, 1640 (C=O), 1605 (C=N); <sup>1</sup>H NMR (700 MHz, DMSO-*d*<sub>6</sub>) δ 10.88 (s, 1H), 10.63 (s, 1H), 8.44 (d, *J* = 8 Hz, 1H), 8.24 (d, *J* = 8 Hz, 1H), 8.03 (m, 2H), 7.83 – 7.74 (m, 2H), 7.73 (s, 1H), 7.63 (t, *J* = 10.3 Hz, 2H), 7.63 – 7.51 (m, 1H), 7.41 – 7.34 (m, 2H), 4.94 (s, 2H), 2.49 (s, 3H); <sup>13</sup>C NMR (176 MHz, DMSO-*d*<sub>6</sub>) δ 165.84, 165.43, 157.96, 154.85, 151.48, 147.63, 146.74, 139.02, 138.28, 133.46, 132.46, 131.23, 131.02, 130.20, 129.28, 125.86, 123.95, 119.16, 118.88, 118.78, 116.21, 115.18, 63.52, 21.58; MS (*m/z*): 431 (M<sup>+</sup> + 1, 30% %), 201 (100%); Anal. Calcd. for C<sub>24</sub>H<sub>19</sub>N<sub>4</sub>O<sub>3</sub> (430.44): C, 66.97; H, 4.45; N, 13.02; Found: C, 66.57; H, 4.34; N, 12.74%.

**4.1.1.9. 4-(2-(3-Methyl-2-oxoquinoxalin-1(2H)-yl)acetamido)-N-(pyridin-2-yl)benzamide 11i.** Buff powder (yield 70%); mp: 292 – 294 °C; FT-IR (ν max, cm<sup>-1</sup>): 3438 (NH), 1660 (C=O), 1600 (C=N); <sup>1</sup>H NMR (700 MHz, DMSO-*d*<sub>6</sub>) δ 10.78 (s, 1H), 8.31 (s, 1H), 7.90 (ddd, *J* = 4.9, 1.9, 0.9 Hz, 1H), 7.89 (td, *J* = 7.7, 2.0 Hz, 1H), 7.80 (dd, *J* = 8.0, 1.5 Hz, 1H), 7.74 – 7.70 (m, 2H), 7.63 – 7.59 (m, 2H), 7.56 (ddd, *J* = 8.6, 7.1, 1.5 Hz, 1H), 7.52 – 7.48 (m, 2H), 7.37 (ddd, *J* = 8.1, 7.2, 1.2 Hz, 1H), 7.27 (ddd, *J* = 7.5, 4.8, 1.0 Hz, 1H), 5.14 (s, 2H), 2.48 (s, 3H); <sup>13</sup>C NMR (176 MHz, DMSO-*d*<sub>6</sub>) δ 172.54, 165.96, 157.95, 154.81, 154.18, 149.22, 142.85, 139.16, 133.41, 132.44, 130.93, 130.19 (2C), 129.56, 129.27, 123.94, 122.89, 122.73, 118.99 (2C), 115.17, 45.81, 21.57; Anal. Calcd. for C<sub>23</sub>H<sub>19</sub>N<sub>5</sub>O<sub>3</sub> (413.44): C, 66.82; H, 4.63; N, 16.94; Found: C, 66.97; H, 4.46; N, 16.79%.

**4.1.1.10. 4-(2-(3-Methyl-2-oxoquinoxalin-1(2H)-yl)acetamido)-N-(thiazol-2-yl)benzamide 11j.** Brown crystals (yield 71%); mp: 230 – 232 °C; FT-IR (ν max, cm<sup>-1</sup>): 3413 (NH), 1660 (C=O), 1602 (C=N); <sup>1</sup>H NMR (700 MHz, DMSO-*d*<sub>6</sub>) δ 12.51 (s, 1H), 10.94 (s, 1H), 8.14 (d, *J* = 8.4 Hz, 1H), 8.10 (d, *J* = 8.7 Hz, 1H), 7.82 – 7.75 (m, 2H), 7.73 (d, *J* = 8.5 Hz, 1H), 7.61 – 7.55 (m, 3H), 7.29 – 7.25 (m, 1H), 7.06 – 7.04 (m, 1H), 5.19 (d, *J* = 6.4 Hz, 2H), 2.49 (s, 3H); <sup>13</sup>C NMR (176 MHz, DMSO-*d*<sub>6</sub>) δ 172.05, 167.52, 166.18, 165.96, 157.97, 142.04, 133.45, 132.14, 130.34, 130.20, 129.85(2C), 129.82, 129.04, 118.90, 118.60(2C), 115.20, 114.21, 108.50, 45.84; MS (*m/z*): 420 (M<sup>+</sup> + 1, 100%); Anal. Calcd. for C<sub>21</sub>H<sub>17</sub>N<sub>5</sub>O<sub>3</sub>S (419.46): C, 60.13; H, 4.09; N, 16.70; Found: C, 60.55; H, 3.68; N, 16.32%.

#### 4.1.2. General procedure for synthesis of compounds 12a-k

To a solution of the potassium salt of 3-methylquinoxaline-2-thiol **4** (352 mg, 0.002 mol) in DMF (20 ml) the appropriate 4-(2-chloroacetamido)-*N*-substituted-benzamides **10a-k** (0.002 mol) was added. The mixture was heated on a water bath for 6 h. After cooling to room temperature, the reaction mixture was poured onto crushed ice. The precipitated solids were filtered, dried, and crystallised from ethanol to give the target compounds **12a-k**.

**4.1.2.1. *N*-Methyl-4-(2-((3-methylquinoxalin-2-yl)thio)acetamido)benzamide 12a.** Brown powder (yield 65%); mp: 219–221 °C; FT-IR (v max, cm<sup>-1</sup>): 3298 (NH), 2923 (CH aliphatic), 1649 (C=O), 1604 (C=N); <sup>1</sup>H NMR (700 MHz, DMSO-*d*<sub>6</sub>) δ 10.71 (s, 1H), 8.38 (q, *J* = 4.6 Hz, 1H), 7.85–7.80 (m, 3H), 7.68 (d, *J* = 8.4 Hz, 2H), 7.59 (t, *J* = 8.4 Hz, 1H), 7.55 (d, *J* = 8.4 Hz, 1H), 7.40 (t, *J* = 7.5 Hz, 1H), 5.19 (s, 2H), 2.79 (s, 3H), 2.30 (s, 3H); <sup>13</sup>C NMR (176 MHz, DMSO) δ 166.48, 165.70, 157.99, 154.86, 141.48, 133.48, 132.47, 130.19, 129.89, 129.28, 128.48 (2C), 123.95, 118.85(2C), 115.20, 45.76, 26.69, 21.61; Anal. Calcd. for C<sub>19</sub>H<sub>18</sub>N<sub>4</sub>O<sub>2</sub>S (366.44): C, 62.28; H, 4.95; N, 15.29; Found: C, 62.53; H, 5.42; N, 15.88%.

**4.1.2.2. *N*-(*sec*-Butyl)-4-(2-((3-methylquinoxalin-2-yl)thio)acetamido)benzamide 12b.** Brown powder (yield 65%); mp: 165–167 °C; FT-IR (v max, cm<sup>-1</sup>): 3286 (NH), 2965 (CH aliphatic), 1631 (C=O), 1608 (C=N); <sup>1</sup>H NMR (700 MHz, DMSO-*d*<sub>6</sub>) δ 10.66 (s, 1H), 8.05 (d, *J* = 8.2 Hz, 1H), 8.02 (d, *J* = 8.2 Hz, 1H), 7.96 (dd, *J* = 8.1, 1.5 Hz, 1H), 7.83 (d, *J* = 8.5 Hz, 2H), 7.82 (s, 1H), 7.72 (d, *J* = 6.9 Hz, 1H), 7.69 (d, *J* = 8.7 Hz, 2H), 4.30 (s, 2H), 3.91 (m, *J* = 7.1 Hz, 2H), 2.67 (s, 3H), 1.51 (dt, *J* = 22.9, 7.2 Hz, 2H), 1.13 (d, *J* = 6.6 Hz, 3H), 0.86 (t, *J* = 7.4 Hz, 3H); <sup>13</sup>C NMR (176 MHz, DMSO-*d*<sub>6</sub>) δ 166.91, 165.53, 155.45, 151.96, 141.86, 140.81, 139.35, 130.09, 130.02, 128.89, 128.67, 128.62(2C), 127.37, 118.65(2C), 46.79, 35.38, 29.34, 22.18, 20.78, 11.24; MS (*m/z*): 409 (M<sup>+</sup> + 1, 100%, base peak); Anal. Calcd. for C<sub>22</sub>H<sub>24</sub>N<sub>4</sub>O<sub>2</sub>S (408.52): C, 64.68; H, 5.92; N, 13.71; Found: C, 64.99; H, 5.77; N, 13.50%.

**4.1.2.3. *N*-Cyclopentyl-4-(2-((3-methylquinoxalin-2-yl)thio)acetamido)benzamide 12c.** Grey powder (yield 72%); mp: 220–222 °C; FT-IR (v max, cm<sup>-1</sup>): 3285 (NH), 2954, 2866 (CH aliphatic), 1668, 1629 (C=O), 1607 (C=N); <sup>1</sup>H NMR (700 MHz, DMSO-*d*<sub>6</sub>) δ 10.66 (s, 1H), 8.15 (d, *J* = 7.2 Hz, 1H), 7.96 (dd, *J* = 8.1, 1.6 Hz, 1H), 7.85–7.80 (m, 3H), 7.71 (ddd, *J* = 8.3, 6.9, 1.6 Hz, 1H), 7.68 (dq, *J* = 9.8, 3.0, 2.2 Hz, 3H), 4.30 (s, 2H), 4.25–4.18 (m, 1H), 2.67 (s, 3H), 1.91–1.84 (m, 2H), 1.74–1.65 (m, 2H), 1.57–1.48 (m, 4H); <sup>13</sup>C NMR (176 MHz, DMSO-*d*<sub>6</sub>) δ 166.91, 165.79, 155.45, 151.97, 141.86, 140.81, 139.35, 130.02, 129.97, 128.90, 128.69, 128.67(2C), 127.37, 118.61(2C), 51.33, 35.38, 32.61(2C), 24.09(2C), 22.18; MS (*m/z*): 421 (M<sup>+</sup> + 1, 100%); Anal. Calcd. for C<sub>23</sub>H<sub>24</sub>N<sub>4</sub>O<sub>2</sub>S (420.53): C, 65.69; H, 5.75; N, 13.32; Found: C, 65.23; H, 5.50; N, 13.02%.

**4.1.2.4. *N*-(2-Methoxyphenyl)-4-(2-((3-methylquinoxalin-2-yl)thio)acetamido)benzamide 12d.** Buff powder (yield 72%); mp: 185–187 °C; FT-IR (v max, cm<sup>-1</sup>): 3420 (NH), 1698, 1645 (C=O), 1602 (C=N); <sup>1</sup>H NMR (700 MHz, DMSO-*d*<sub>6</sub>) δ 10.75 (s, 1H), 9.31 (s, 1H), 7.99–7.93 (m, 3H), 7.85–7.82 (m, 1H), 7.80 (dd, *J* = 7.8, 1.6 Hz, 1H), 7.78–7.75 (m, 2H), 7.71 (dddd, *J* = 25.1, 8.4, 7.0, 1.5 Hz, 2H), 7.18 (ddd, *J* = 8.2, 7.4, 1.7 Hz, 1H), 7.10 (dd, *J* = 8.3, 1.3 Hz, 1H), 6.97 (td, *J* = 7.6, 1.4 Hz, 1H), 4.33 (s, 2H), 3.84 (s, 3H), 2.68 (s, 3H); <sup>13</sup>C NMR (176 MHz, DMSO-*d*<sub>6</sub>) δ 167.07, 164.77, 155.46, 151.98, 151.77, 142.51, 140.82, 139.36, 130.06, 129.49, 128.99, 128.92(2C), 128.69, 127.41, 127.38, 125.97, 124.53, 120.67, 118.88(2C), 111.80, 56.19, 35.44, 22.19; MS (*m/z*): 459 (M<sup>+</sup> + 1,

70% %), 217 (100%); Anal. Calcd. for C<sub>25</sub>H<sub>22</sub>N<sub>4</sub>O<sub>3</sub>S (458.54): C, 65.49; H, 4.84; N, 12.22; Found: C, 65.11; H, 4.62; N, 12.56%.

**4.1.2.5. *N*-(3-Methoxyphenyl)-4-(2-((3-methylquinoxalin-2-yl)thio)acetamido)benzamide 12e.** Reddish crystals (yield 70%); mp: 232–234 °C; FT-IR (v max, cm<sup>-1</sup>): 3277 (NH), 3039 (CH aromatic), 2989, 2926, 2827 (CH aliphatic), 1678, 1650 (C=O); <sup>1</sup>H NMR (700 MHz, DMSO-*d*<sub>6</sub>) δ 10.76 (s, 1H), 10.11 (s, 1H), 7.96 (d, *J* = 8.7 Hz, 3H), 7.83 (dd, *J* = 8.2, 1.5 Hz, 1H), 7.80–7.76 (m, 2H), 7.70 (dddd, *J* = 25.4, 8.4, 6.9, 1.5 Hz, 2H), 7.48 (t, *J* = 2.3 Hz, 1H), 7.40–7.35 (m, 1H), 7.25 (t, *J* = 8.1 Hz, 1H), 6.70–6.65 (m, 1H), 4.33 (s, 2H), 3.76 (s, 3H), 2.67 (s, 3H); <sup>13</sup>C NMR (176 MHz, DMSO-*d*<sub>6</sub>) δ 167.08, 165.36, 159.88, 155.43, 151.96, 142.49, 140.94, 140.82, 139.36, 130.02, 129.90, 129.81, 129.19 (2C), 128.89, 128.68, 127.37, 118.78 (2C), 112.97, 109.46, 106.44, 55.45, 35.44, 22.18; MS (*m/z*): 459 (M<sup>+</sup> + 1, 100%); Anal. Calcd. for C<sub>25</sub>H<sub>22</sub>N<sub>4</sub>O<sub>3</sub>S (458.54): C, 65.49; H, 4.84; N, 12.22; Found: C, 65.83; H, 4.57; N, 11.94%.

**4.1.2.6. *N*-(4-Methoxyphenyl)-4-(2-((3-methylquinoxalin-2-yl)thio)acetamido)benzamide 12f.** White powder (yield 71%); mp: 250–252 °C; FT-IR (v max, cm<sup>-1</sup>): 3300 (NH), 3054 (CH aromatic), 2909, 2834 (CH aliphatic), 1677, 1644 (C=O), 1600 (C=N); <sup>1</sup>H NMR (700 MHz, DMSO-*d*<sub>6</sub>) δ 10.74 (s, 1H), 10.02 (s, 1H), 7.96 (t, *J* = 9.1 Hz, 3H), 7.83 (dd, *J* = 8.0, 2.8 Hz, 1H), 7.76 (dd, *J* = 8.6, 2.9 Hz, 2H), 7.72 (t, *J* = 7.5 Hz, 1H), 7.67 (dd, *J* = 9.1, 3.1 Hz, 3H), 6.93 (dd, *J* = 9.2, 3.0 Hz, 2H), 4.33 (s, 2H), 3.75 (s, 3H), 2.67 (d, *J* = 2.9 Hz, 3H); <sup>13</sup>C NMR (176 MHz, DMSO-*d*<sub>6</sub>) δ 167.04, 164.91, 155.91, 155.45, 151.97, 142.30, 140.82, 139.36, 132.79, 130.03 (2C), 129.05 (2C), 128.89, 128.68, 127.37, 122.40 (2C), 118.77 (2C), 114.18 (2C), 55.63, 35.43, 22.18; MS (*m/z*): 459 (M<sup>+</sup> + 1, 100%); Anal. Calcd. for C<sub>25</sub>H<sub>22</sub>N<sub>4</sub>O<sub>3</sub>S (458.54): C, 65.49; H, 4.84; N, 12.22; Found: C, 65.02; H, 4.57; N, 11.99%.

**4.1.2.7. *N*-(4-Acetylphenyl)-4-(2-((3-methylquinoxalin-2-yl)thio)acetamido)benzamide 12g.** Brown powder (yield 77%); mp: 270–273 °C; FT-IR (v max, cm<sup>-1</sup>): 3300 (NH), 2918 (CH aliphatic), 1672, 1649 (C=O), 1590 (C=N); <sup>1</sup>H NMR (700 MHz, DMSO-*d*<sub>6</sub>) δ 10.78 (s, 1H), 10.45 (s, 1H), 7.99 (d, *J* = 2.3 Hz, 1H), 7.98 (d, *J* = 2.4 Hz, 2H), 7.97 (d, *J* = 1.9 Hz, 2H), 7.95 (s, 1H), 7.94 (d, *J* = 2.0 Hz, 1H), 7.83 (dd, *J* = 8.1, 1.6 Hz, 1H), 7.80 (d, *J* = 2.0 Hz, 1H), 7.79 (d, *J* = 1.9 Hz, 1H), 7.72 (ddd, *J* = 8.3, 6.9, 1.6 Hz, 1H), 7.68 (ddd, *J* = 8.3, 6.9, 1.6 Hz, 1H), 4.33 (s, 2H), 2.67 (s, 3H), 2.55 (s, 3H); <sup>13</sup>C NMR (176 MHz, DMSO-*d*<sub>6</sub>) δ 197.05, 167.14, 165.74, 155.43, 151.97, 144.22, 142.79, 140.81, 139.36, 132.33, 130.03, 129.76 (2C), 129.43(2C), 128.90, 128.69, 127.37, 119.84, 119.82(2C), 118.81(2C), 35.44, 26.93, 22.18; MS (*m/z*): 471 (M<sup>+</sup> + 1, 100%); Anal. Calcd. for C<sub>26</sub>H<sub>22</sub>N<sub>4</sub>O<sub>3</sub>S (470.55): C, 66.37; H, 4.71; N, 11.91; Found: C, 65.94; H, 4.66; N, 11.58%.

**4.1.2.8. *N*-(4-Fluorophenyl)-4-(2-((3-methylquinoxalin-2-yl)thio)acetamido)benzamide 12h.** White powder (yield 72%); mp: 250–252 °C; FT-IR (v max, cm<sup>-1</sup>): 3261 (NH), 3042 (CH aromatic), 2912 (CH aliphatic), 1659, 1640 (C=O), 1608 (C=N); <sup>1</sup>H NMR (700 MHz, DMSO-*d*<sub>6</sub>) δ 10.77 (s, 1H), 10.20 (s, 1H), 7.96 (d, *J* = 8.9 Hz, 3H), 7.83 (d, *J* = 8.1 Hz, 1H), 7.79 (t, *J* = 9.1 Hz, 4H), 7.74–7.65 (m, 2H), 7.19 (t, *J* = 8.7 Hz, 2H), 4.33 (s, 2H), 2.67 (s, 3H); <sup>13</sup>C NMR (176 MHz, DMSO-*d*<sub>6</sub>) δ 167.08, 165.26, 155.43, 151.96, 142.52, 140.82, 139.36, 130.01, 129.72, 129.17(2C), 128.88, 128.68, 127.37, 122.60(2C), 122.56, 118.80(2C), 115.67(2C), 115.54, 35.43, 22.18; MS (*m/z*): 447 (M<sup>+</sup> + 1, 70% %); Anal. Calcd. for C<sub>24</sub>H<sub>19</sub>FN<sub>4</sub>O<sub>2</sub>S (446.50): C, 64.56; H, 4.29; F, 4.25; N, 12.55; Found: C, 64.12; H, 3.83; N, 12.14%.

**4.1.2.9. 4-(2-((3-Methylquinoxalin-2-yl)thio)acetamido)-N-(pyridin-2-yl)benzamide 12i.** Grey powder (yield 70%); mp: 215–217 °C; FT-IR (v max, cm<sup>-1</sup>): 3311 (NH), 1683 (C=O), 1593 (C=N); <sup>1</sup>H NMR (700 MHz, DMSO-*d*<sub>6</sub>) δ 10.77 (s, 1H), 10.20 (s, 1H), 8.30 (ddd, *J*=4.8, 1.9, 0.8 Hz, 1H), 7.96 (dd, *J*=8.0, 1.7 Hz, 1H), 7.88 (td, *J*=7.8, 2.0 Hz, 1H), 7.81–7.77 (m, 1H), 7.73–7.71 (m, 2H), 7.69 (td, *J*=7.8, 1.6 Hz, 2H), 7.67–7.65 (m, 2H), 7.49 (dt, *J*=8.1, 1.0 Hz, 1H), 7.26 (ddd, *J*=7.4, 4.8, 1.0 Hz, 1H), 4.29 (s, 2H), 2.66 (s, 3H); <sup>13</sup>C NMR (176 MHz, DMSO-*d*<sub>6</sub>) δ 172.58, 167.24, 155.37, 154.21, 151.94, 149.20, 143.34, 140.78, 139.35, 139.15, 130.95, 130.04, 129.28, 128.92 (2C), 128.67, 127.37, 122.84, 122.68, 118.94 (2C), 35.42, 22.17; MS (*m/z*): 430 (M<sup>+</sup> + 1, 80%), 119 (100%); Anal. Calcd. for C<sub>23</sub>H<sub>19</sub>N<sub>5</sub>O<sub>2</sub>S (429.50): C, 64.32; H, 4.46; N, 16.31; Found: C, 64.61; H, 4.84; N, 15.92%.

**4.1.2.10. 4-(2-((3-Methylquinoxalin-2-yl)thio)acetamido)-N-(*m*-tol-yl)benzamide 12j.** Buff powder (yield 73%); mp: 242–244 °C; FT-IR (v max, cm<sup>-1</sup>): 3287 (NH), 1674, 1643 (C=O), 1591 (C=N); <sup>1</sup>H NMR (700 MHz, DMSO-*d*<sub>6</sub>) δ 10.74 (s, 1H), 10.05 (s, 1H), 7.99–7.93 (m, 3H), 7.84 (dd, *J*=8.1, 1.6 Hz, 1H), 7.79–7.75 (m, 2H), 7.71 (dddd, *J*=24.1, 8.3, 7.0, 1.5 Hz, 2H), 7.61 (t, *J*=2.0 Hz, 1H), 7.58–7.54 (m, 1H), 7.23 (t, *J*=7.8 Hz, 1H), 6.94–6.90 (m, 1H), 4.33 (s, 2H), 2.68 (s, 3H), 2.31 (s, 3H); <sup>13</sup>C NMR (176 MHz, DMSO-*d*<sub>6</sub>) δ 167.06, 165.25, 155.45, 151.98, 142.42, 140.82, 139.65, 139.36, 138.16, 130.04, 129.96, 129.16 (2C), 128.92, 128.88, 128.69, 127.38, 124.67, 121.33, 118.77 (2C), 117.97, 35.43, 22.19, 21.70; MS (*m/z*): 443 (M<sup>+</sup> + 1, 100%); Anal. Calcd. for C<sub>25</sub>H<sub>22</sub>N<sub>4</sub>O<sub>2</sub>S (442.54): C, 67.85; H, 5.01; N, 12.66; Found: C, 67.53; H, 4.94; N, 12.38%.

**4.1.2.11. 4-(2-((3-Methylquinoxalin-2-yl)thio)acetamido)-N-(*p*-tolyl)-benzamide 12k.** White powder (yield 77%); mp: 259–261 °C; FT-IR (v max, cm<sup>-1</sup>): 3291, (NH), 3036 (CH aromatic), 2982, 2922 (CH aliphatic), 1661, 1641 (C=O), 1596 (C=N); <sup>1</sup>H NMR (700 MHz, DMSO-*d*<sub>6</sub>) δ 10.74 (s, 1H), 10.05 (s, 1H), 7.96 (dd, *J*=10.2, 8.4 Hz, 3H), 7.83 (dd, *J*=8.1, 1.5 Hz, 1H), 7.77 (d, *J*=8.5 Hz, 2H), 7.73–7.70 (m, 1H), 7.68 (ddd, *J*=8.3, 7.0, 1.5 Hz, 1H), 7.65 (d, *J*=8.2 Hz, 2H), 7.15 (d, *J*=8.2 Hz, 2H), 4.33 (s, 2H), 2.67 (s, 3H), 2.28 (s, 3H); <sup>13</sup>C NMR (176 MHz, DMSO-*d*<sub>6</sub>) δ 167.05, 165.13, 155.45, 151.97, 142.37, 140.82, 139.36, 137.20, 132.90, 130.03, 130.01, 129.43(2C), 129.12 (2C), 128.90, 128.68, 127.37, 120.81 (2C), 118.77 (2C), 35.43, 22.19, 20.96; MS (*m/z*): 443 (M<sup>+</sup> + 1, 100%); Anal. Calcd. for C<sub>25</sub>H<sub>22</sub>N<sub>4</sub>O<sub>2</sub>S (442.54): C, 67.85; H, 5.01; N, 12.66; Found: C, 67.45; H, 4.89; N, 12.21%.

## 4.2. Biological testing

### 4.2.1. In vitro cytotoxic activity

*In vitro* cytotoxicity was carried out using MTT assay protocol<sup>47,65–67</sup> as described in Supplementary data.

### 4.2.2. In vitro VEGFR-2 kinase assay

*In vitro* VEGFR-2 inhibitory activity was assessed against Human VEGFR-2 ELISA kit as described in Supplementary data<sup>68,69</sup>.

### 4.2.3. In vitro cytotoxicity against normal cell

The toxicity of compounds **11e** and **12e** was assessed against normal cell lines (primary rat hepatocytes) according to method of two-steps *in situ* collagenase perfusion as described by Seglen<sup>70</sup> (Supplementary data).

### 4.2.4. Cell cycle analysis

The effect of compound **11e** on cell cycle distribution was performed using propidium iodide (PI) staining technique as described in Supplementary data<sup>71–73</sup>.

### 4.2.5. Apoptosis analysis

The effect of compound **11e** on cell apoptosis was investigated as described in Supplementary data<sup>74–76</sup>.

### 4.2.6. Western blot analysis

Western blot technique was applied to assess the potential effect of compound **11e** on the expression of caspase-9, caspase-3, BAX, and Bcl-2 as reported in Supplementary data<sup>77–79</sup>.

## 4.3. In silico studies

### 4.3.1. Docking studies

Crystal structure of VEGFR-2 [PDB ID: PDB ID: 2OH4, resolution: 2.05 Å] was obtained from Protein Data Bank. The docking investigation was accomplished using MOE2014 software. At first, the crystal structure of VEGFR-2 was prepared by removing water molecules. Only one chain was retained beside the co-crystallized ligand (sorafenib). Then, the selected chain was protonated and subjected to minimisation of energy process. Next, the active site of the target protein was defined.

Structures of the synthesised compounds and sorafenib were drawn using ChemBioDraw Ultra 14.0 and saved as MDL-SD format. Such file was opened using MOE to display the 3D structures which were protonated and subjected to energy minimisation. Formerly, validation of the docking process was performed by docking the co-crystallized ligand against the isolated pocket of active site. The produced RMSD value indicated the validity of process. Finally, docking of the tested compounds was done through the dock option inserted in compute window. For each docked molecule, 30 docked poses were produced using ASE for scoring function and force field for refinement. The results of the docking process were then visualised using Discovery Studio 4.0 software<sup>34,80–83</sup>.

### 4.3.2. ADMET studies

ADMET descriptors were determined using Discovery studio 4.0 as according the reported method<sup>34,80,84</sup> (Supplementary data).

### 4.3.3. Toxicity studies

Discovery studio 4.0 software was used to predict the toxicity potential of the synthesised compounds as reported in Supplementary data<sup>85</sup>.

## Acknowledgements

The authors extend their appreciation to the Deanship of Scientific Research at King Saud University for funding this work through research group no (RG-1441–333).

## Disclosure statement

There is no any conflict of interest. Authors thank Dr. Mohamad Elnagar, Pharmacology and Toxicology Department, Faculty of



Pharmacy, Al-Azhar University, Cairo, Egypt for his support in biological testing.

## Funding

The authors extend their appreciation to the Deanship of Scientific Research at King Saud University for funding this work through research group no (RG-1441-333).

## ORCID

Mohammed M. Alanazi  <http://orcid.org/0000-0002-0483-8113>

Elwan Alaa  <http://orcid.org/0000-0003-4270-616X>

Nawaf A. Alsaif  <http://orcid.org/0000-0001-9215-1380>

Ahmad J. Obaidullah  <http://orcid.org/0000-0002-7532-6318>

Hamad M. Alkahtani  <http://orcid.org/0000-0002-6983-8587>

Abdulrahman A. Al-Mehizia  <http://orcid.org/0000-0002-6824-0137>

Mohammed S. Taghour  <http://orcid.org/0000-0003-0630-709X>

Ibrahim H. Eissa  <http://orcid.org/0000-0002-6955-2263>

## References

- Baselga J, Bhardwaj N, Cantley LC, et al. AACR cancer progress report 2015. *Clin Cancer Res* 2015;21:S1–S128.
- Daher IN, Daigle TR, Bhatia N, Durand J-B. The prevention of cardiovascular disease in cancer survivors. *Tex Heart Inst J* 2012;39:190–8.
- WHO. Cancer. Available from: [https://www.who.int/health-topics/cancer#tab=tab\\_1](https://www.who.int/health-topics/cancer#tab=tab_1). [accessed May 2020].
- DE, Thurston Chemistry and pharmacology of anticancer drugs. 2nd ed. Boca Raton, FL: CRC Press; 2006.
- Roskoski R. Jr, The ErbB/HER family of protein-tyrosine kinases and cancer. *Pharmacol Res* 2014;79:34–74.
- Blume-Jensen P, Hunter T. Oncogenic kinase signalling. *Nature* 2001;411:355–65.
- Schlessinger J. Cell signaling by receptor tyrosine kinases. *Cell* 2000;103:211–25.
- Modi SJ, Kulkarni VM. Vascular Endothelial Growth Factor Receptor (VEGFR-2)/KDR inhibitors: medicinal chemistry perspective. *Med Drug Discov* 2019;2:100009.
- Mahdy HA, Ibrahim MK, Metwaly AM, et al. Design, synthesis, molecular modeling, in vivo studies and anticancer evaluation of quinazolin-4(3H)-one derivatives as potential VEGFR-2 inhibitors and apoptosis inducers. *Bioorg Chem* 2020;94:103422
- El-Adl K, El-Helby A-GA, Sakr H, et al. Design, synthesis, molecular docking and anticancer evaluations of 5-benzylidenethiazolidine-2, 4-dione derivatives targeting VEGFR-2 enzyme. *Bioorg Chem* 2020;102:104059.
- Olsson A-K, Dimberg A, Kreuger J, Claesson-Welsh L. VEGF receptor signalling - in control of vascular function. *Nat Rev Mol Cell Biol* 2006;7:359–71.
- Melincovici CS, Boşca AB, Şuşman S, et al. Vascular endothelial growth factor (VEGF)-key factor in normal and pathological angiogenesis. *Rom J Morphol Embryol* 2018;59:455–67.
- Padro T, Bieker R, Ruiz S, et al. Overexpression of vascular endothelial growth factor (VEGF) and its cellular receptor KDR (VEGFR-2) in the bone marrow of patients with acute myeloid leukemia. *Leukemia* 2002;16:1302–10.
- Yang C, Qin S. Apatinib targets both tumor and endothelial cells in hepatocellular carcinoma. *Cancer Med* 2018;7:4570–83.
- Guo S, Colbert LS, Fuller M, et al. Vascular endothelial growth factor receptor-2 in breast cancer. *Biochim Biophys Acta* 2010;1806:108–21.
- Martins SF, Garcia EA, LUZ MAM, et al. Clinicopathological correlation and prognostic significance of VEGF-A, VEGF-C, VEGFR-2 and VEGFR-3 expression in colorectal cancer. *Cancer Genomics Proteomics* 2013;10:55–67.
- Holmes K, Roberts OL, Thomas AM, Cross MJ. Vascular endothelial growth factor receptor-2: structure, function, intracellular signalling and therapeutic inhibition. *Cell Signal* 2007;19:2003–12.
- Morabito A, De Maio E, Maio MD, et al. Tyrosine kinase inhibitors of vascular endothelial growth factor receptors in clinical trials: current status and future directions. *Oncologist* 2006;11:753–64.
- Chow LQ, Eckhardt SG. Sunitinib: from rational design to clinical efficacy. *J Clin Oncol* 2007;25:884–96.
- Steehgs N, Gelderblom H, Wessels J, et al. Pharmacogenetics of telatinib, a VEGFR-2 and VEGFR-3 tyrosine kinase inhibitor, used in patients with solid tumors. *Invest New Drugs* 2011;29:137–43.
- Roth GJ, Binder R, Colbatzky R, et al. Nintedanib: from discovery to the clinic. Washington, DC: ACS Publications; 2015.
- Adams CM, Anderson K, Artman Iii G, et al. The Discovery of N-(1-Methyl-5-(trifluoromethyl)-1-H-pyrazol-3-yl)-5-((methylamino) methyl) pyrimidin-4-yl) oxy)-1 H-indole-1-carboxamide (Acrizatinib), a VEGFR-2 inhibitor specifically designed for topical ocular delivery, as a therapy for neovascular age-related macular degeneration. *J Med Chem* 2018;61:1622–35.
- Sheng X, Yan X, Tang B, et al. A phase I clinical trial of CM082 (X-82) in combination with everolimus for treatment of metastatic renal cell carcinoma. *Am Soc Clin Oncol* 2017;35:4575–5.
- Moore KN, Jones SF, Kurkjian C, et al. Phase I, first-in-human trial of an oral VEGFR tyrosine kinase inhibitor (TKI) x-82 in patients (pts) with advanced solid tumors. *Am Soc Clin Oncol* 2012;30:3041.
- Xie Q-Q, Xie H-Z, Ren J-X, et al. Pharmacophore modeling studies of type I and type II kinase inhibitors of Tie2. *J Mol Graph Model* 2009;27:751–8.
- Lee K, Jeong K-W, Lee Y, et al. Pharmacophore modeling and virtual screening studies for new VEGFR-2 kinase inhibitors. *Eur J Med Chem* 2010;45:5420–7.
- Eskander RN, Tewari KS. Incorporation of anti-angiogenesis therapy in the management of advanced ovarian carcinoma-mechanistics, review of phase III randomized clinical trials, and regulatory implications. *Gynecol Oncol* 2014;132:496–505.
- Eissa IH, Ibrahim MK, Metwaly AM, et al. Design, molecular docking, in vitro, and in vivo studies of new quinazolin-4(3H)-ones as VEGFR-2 inhibitors with potential activity against hepatocellular carcinoma. *Bioorg Chem* 2021;107:104532.
- El-Metwally SA, Abou-El-Regal MM, Eissa IH, et al. Discovery of thieno[2,3-d]pyrimidine-based derivatives as potent VEGFR-2 kinase inhibitors and anti-cancer agents. *Bioorg Chem* 2021;112:104947.
- Alsaif NA, Dahab MA, Alanazi MM, et al. New quinoxaline derivatives as VEGFR-2 inhibitors with anticancer and

- apoptotic activity: design, molecular modeling, and synthesis. *Bioorg Chem* 2021;110:104807.
31. Machado VA, Peixoto D, Costa R, et al. Synthesis, antiangiogenesis evaluation and molecular docking studies of 1-aryl-3-[(thieno[3,2-b]pyridin-7-ylthio)phenyl]ureas: discovery of a new substitution pattern for type II VEGFR-2 Tyr kinase inhibitors. *Bioorg Med Chem* 2015;23:6497–509.
  32. Wang Z, Wang N, Han S, et al. Dietary compound isoliquiritigenin inhibits breast cancer neoangiogenesis via VEGF/VEGFR-2 signaling pathway. *PLoS One* 2013;8:e68566.
  33. Dietrich J, Hulme C, Hurley LH. The design, synthesis, and evaluation of 8 hybrid DFG-out allosteric kinase inhibitors: a structural analysis of the binding interactions of Gleevec, Nexavar, and BIRB-796. *Bioorg Med Chem* 2010;18:5738–48.
  34. Ibrahim MK, Eissa IH, Alesawy MS, et al. Design, synthesis, molecular modeling and anti-hyperglycemic evaluation of quinazolin-4(3H)-one derivatives as potential PPAR $\gamma$  and SUR agonists. *Bioorg Med Chem* 2017;25:4723–44.
  35. Eldehna WM, Abo-Ashour MF, Nocentini A, et al. Novel 4/3-((4-oxo-5-(2-oxoindolin-3-ylidene)thiazolidin-2-ylidene)amino)benzenesulfonamides: synthesis, carbonic anhydrase inhibitory activity, anticancer activity and molecular modelling studies. *Eur J Med Chem* 2017;139:250–62.
  36. El-Zahabi MA, Sakr H, El-Adl K, et al. Design, synthesis, and biological evaluation of new challenging thalidomide analogs as potential anticancer immunomodulatory agents. *Bioorg Chem* 2020;104:104218.
  37. Nasser AA, Eissa IH, Oun MR, et al. Discovery of new pyrimidine-5-carbonitrile derivatives as anticancer agents targeting EGFRWT and EGFR790M. *Org Biomol Chem* 2020;18:7608–34.
  38. El-Helby AGA, Sakr H, Eissa IH, et al. Benzoxazole/benzothiazole-derived VEGFR-2 inhibitors: design, synthesis, molecular docking, and anticancer evaluations. *Archiv Der Pharmazie* 2019;352:1900178.
  39. El-Helby AGA, Sakr H, Eissa IH, et al. Design, synthesis, molecular docking, and anticancer activity of benzoxazole derivatives as VEGFR-2 inhibitors. *Archiv Der Pharmazie* 2019;352:1900113.
  40. Zhang L, Shan Y, Ji X, et al. Discovery and evaluation of triple inhibitors of VEGFR-2, TIE-2 and EphB4 as anti-angiogenic and anti-cancer agents. *Oncotarget* 2017;8:104745–60.
  41. Abdel-Mohsen HT, Abdullaziz MA, Kerdawy AME, et al. Targeting receptor tyrosine kinase VEGFR-2 in hepatocellular cancer: rational design, synthesis and biological evaluation of 1, 2-disubstituted benzimidazoles. *Molecules* 2020;25:770.
  42. Rampogu S, Baek A, Park C, et al. Discovery of small molecules that target vascular endothelial growth factor receptor-2 signalling pathway employing molecular modelling studies. *Cells* 2019;8:269.
  43. Hou T, Zhu L, Chen L, Xu X. Mapping the binding site of a large set of quinazoline type EGF-R inhibitors using molecular field analyses and molecular docking studies. *J Chem Inf Comput Sci* 2003;43:273–87.
  44. Ibrahim M-K, Abd-Elrahman AA, Ayyad RR, et al. Design and synthesis of some novel 2-(3-methyl-2-oxoquinoxalin-1 (2H)-yl)-N-(4-(substituted) phenyl) acetamide derivatives for biological evaluation as anticonvulsant agents. *Bull Fac Pharm Cairo Univ* 2013;51:101–11.
  45. Saoudi B, Teniou A, Debache A, et al. Cyclisation reaction between 3-methylquinoxaline-2-thione and benzaldehydes into 3-benzyl-2-aryl-thieno [2, 3-b] quinoxaline promoted by Brønsted acids. *Comptes Rendus Chimie* 2015;18:808–15.,
  46. Morrison D, Furst A. Quinoxaline-2-thiols. *J Org Chem* 1956;21:470–1.
  47. Mosmann T. Rapid colorimetric assay for cellular growth and survival: application to proliferation and cytotoxicity assays. *J Immunol Methods* 1983;65:55–63.
  48. Vermeulen K, Berneman ZN, Van Bockstaele DR. Cell cycle and apoptosis. *Cell Prolif* 2003;36:165–75.
  49. Naseri MH, Mahdavi M, Davoodi J, et al. Up regulation of Bax and down regulation of Bcl2 during 3-NC mediated apoptosis in human cancer cells. *Cancer Cell Int* 2015;15:55.
  50. Slee EA, Harte MT, Kluck RM, et al. Ordering the cytochrome c-initiated caspase cascade: hierarchical activation of caspases-2, -3, -6, -7, -8, and -10 in a caspase-9-dependent manner. *J Cell Biol* 1999;144:281–92.
  51. Brentnall M, Rodriguez-Menocal L, De Guevara RL, et al. Caspase-9, caspase-3 and caspase-7 have distinct roles during intrinsic apoptosis. *BMC Cell Biol* 2013;14:32.
  52. Antonsson B, Conti F, Ciavatta A, et al. Inhibition of Bax channel-forming activity by Bcl-2. *Science* 1997;277:370–2.
  53. Perlman H, Zhang X, Chen MW, et al. An elevated bax/bcl-2 ratio corresponds with the onset of prostate epithelial cell apoptosis. *Cell Death Differ* 1999;6:48–54.
  54. Liu Y, Gray NS. Rational design of inhibitors that bind to inactive kinase conformations. *Nat Chem Biol* 2006;2:358–64.
  55. Roy PP, Roy K. QSAR studies of CYP2D6 inhibitor aryloxypropanolamines using 2D and 3D descriptors. *Chem Biol Drug Des* 2009;73:442–55.
  56. Ghafourian T, Amin Z. QSAR models for the prediction of plasma protein binding. *BiolImpacts* 2013;3:21.
  57. Xia X, Maliski EG, Gallant P, Rogers D. Classification of kinase inhibitors using a Bayesian model. *J Med Chem* 2004;47:4463–70.
  58. BIOVIA, QSAR, ADMET and Predictive Toxicology. <https://www.3dsbiovia.com/products/collaborative-science/biovia-discovery-studio/qsar-admet-and-predictive-toxicology.html> [Accessed May 2020].
  59. Eissa IH, El-Helby A-GA, Mahdy HA, et al. Discovery of new quinazolin-4 (3H)-ones as VEGFR-2 inhibitors: design, synthesis, and anti-proliferative evaluation. *Bioorg Chem* 2020;105:104380.
  60. El-Helby A-GA, Sakr H, Ayyad RR, et al. Design, synthesis, molecular modeling, in vivo studies and anticancer activity evaluation of new phthalazine derivatives as potential DNA intercalators and topoisomerase II inhibitors. *Bioorg Chem* 2020;103:104233.
  61. Kanhed AA, Mehre AP, Pandey KR, Mahapatra DK. Mahapatra, 4-(2-chloroacetamido) Benzoic acid derivatives as local anesthetic agents: design, synthesis, and characterization. *UK J Pharm Biosci* 2016;4:35–44.
  62. Alanazi MM, Mahdy HA, Alsaif NA, et al. New bis ([1, 2, 4] triazolo)[4, 3-a: 3', 4'-c] quinoxaline derivatives as VEGFR-2 inhibitors and apoptosis inducers: design, synthesis, in silico studies, and anticancer evaluation. *Bioorg Chem* 2021;112:104949.
  63. Alsaif MSTNA, Alanazi MM, Obaidullah AJ, et al. Discovery of new VEGFR-2 inhibitors based on bis([1, 2, 4]triazolo)[4,3-a:3',4'-c]quinoxaline derivatives as anticancer agents and apoptosis inducers. *J Enzyme Inhib Med Chem* 2021;36:1093–114.
  64. Abbass EM, Khalil AK, Mohamed MM, et al. Design, efficient synthesis, docking studies, and anticancer evaluation of new quinoxalines as potential intercalative Topo II inhibitors and apoptosis inducers. *Bioorg Chem* 2020;104:104255.

65. Denizot F, Lang R. Rapid colorimetric assay for cell growth and survival. Modifications to the tetrazolium dye procedure giving improved sensitivity and reliability. *J Immunol Methods* 1986;89:271–7.
66. Thabrew MI, Hughes RD, Mcfarlane IG. Screening of hepatoprotective plant components using a HepG2 cell cytotoxicity assay. *J Pharm Pharmacol* 2011;49:1132–5.
67. Al-Rashood ST, Hamed AR, Hassan GS, et al. Antitumor properties of certain spirooxindoles towards hepatocellular carcinoma endowed with antioxidant activity. *J Enzyme Inhib Med Chem* 2020;35:831–9.
68. Abou-Seri SM, Eldehna WM, Ali MM, Abou El Ella DA. 1-Piperazinyolphthalazines as potential VEGFR-2 inhibitors and anticancer agents: synthesis and in vitro biological evaluation. *Eur J Med Chem* 2016;107:165–79.
69. Sharma K, Suresh P, Mullangi R, Srinivas N. Quantitation of VEGFR2 (vascular endothelial growth factor receptor) inhibitors-review of assay methodologies and perspectives. *Biomed Chromatogr* 2015;29:803–34.
70. Seglen PO. Preparation of isolated rat liver cells. *Methods Cell Biol* 1976;13:29–83.
71. Wang J, Lenardo MJ. Roles of caspases in apoptosis, development, and cytokine maturation revealed by homozygous gene deficiencies. *J Cell Sci* 2000;113:753–7.
72. Eldehna WM, Hassan GS, Al-Rashood ST, et al. Synthesis and in vitro anticancer activity of certain novel 1-(2-methyl-6-arylpyridin-3-yl)-3-phenylureas as apoptosis-inducing agents. *J Enzyme Inhib Med Chem* 2019;34:322–32.
73. Al-Warhi T, Abo-Ashour MF, Almahli H, et al. Novel [(N-alkyl-3-indolylmethylene)hydrazono]oxindoles arrest cell cycle and induce cell apoptosis by inhibiting CDK2 and Bcl-2: synthesis, biological evaluation and in silico studies. *J Enzyme Inhib Med Chem* 2020;35:1300–9.
74. Lo KK-W, Lee TK-M, Lau JS-Y, et al. Luminescent biological probes derived from ruthenium(II) estradiol polypyridine complexes. *Inorg Chem* 2008;47:200–8.
75. Sabt A, Abdelhafez OM, El-Haggar RS, et al. Novel coumarin-6-sulfonamides as apoptotic anti-proliferative agents: synthesis, in vitro biological evaluation, and QSAR studies. *J Enzyme Inhib Med Chem* 2018;33:1095–107.
76. Al-Sanea MM, Al-Ansary GH, Elsayed ZM, et al. Development of 3-methyl/3-(morpholinomethyl)benzofuran derivatives as novel antitumor agents towards non-small cell lung cancer cells. *J Enzyme Inhib Med Chem* 2021;36:987–99.
77. Balah A, Ezzat O, Akool E-S. Vitamin E inhibits cyclosporin A-induced CTGF and TIMP-1 expression by repressing ROS-mediated activation of TGF- $\beta$ /Smad signaling pathway in rat liver. *Int Immunopharmacol* 2018;65:493–502.
78. Aborehab NM, Elnagar MR, Waly NE. Gallic acid potentiates the apoptotic effect of paclitaxel and carboplatin via overexpression of Bax and P53 on the MCF-7 human breast cancer cell line. *J Biochem Mol Toxicol* 2021;35:e22638.
79. Elnagar MR, Walls AB, Helal GK, et al. Functional characterization of  $\alpha$ 7 nicotinic acetylcholine and NMDA receptor signaling in SH-SY5Y neuroblastoma cells in an ERK phosphorylation assay. *Eur J Pharmacol* 2018;826:106–13.
80. El-Zahabi MA, Elbendary ER, Bamanie FH, et al. Design, synthesis, molecular modeling and anti-hyperglycemic evaluation of phthalimide-sulfonylurea hybrids as PPAR $\gamma$  and SUR agonists. *Bioorg Chem* 2019;91:103115.
81. Ibrahim MK, Eissa IH, Abdallah AE, et al. Design, synthesis, molecular modeling and anti-hyperglycemic evaluation of novel quinoxaline derivatives as potential PPAR $\gamma$  and SUR agonists. *Bioorg Med Chem* 2017;25:1496–513.
82. El-Gamal KM, El-Morsy AM, Saad AM, et al. Synthesis, docking, QSAR, ADMET and antimicrobial evaluation of new quinoline-3-carbonitrile derivatives as potential DNA-gyrase inhibitors. *J Mol Struct* 2018;1166:15–33.
83. El-Naggar AM, Eissa IH, Belal A, El-Sayed AA. Design, eco-friendly synthesis, molecular modeling and anticancer evaluation of thiazol-5 (4H)-ones as potential tubulin polymerization inhibitors targeting the colchicine binding site. *RSC Adv* 2020;10:2791–811.
84. El-Demerdash A, Metwaly AM, Hassan A, et al. Comprehensive virtual screening of the antiviral potentialities of marine polycyclic guanidine alkaloids against SARS-CoV-2 (COVID-19). *Biomolecules* 2021;11:460.
85. Eissa IH, Dahab MA, Ibrahim MK, et al. Design and discovery of new antiproliferative 1, 2, 4-triazin-3 (2H)-ones as tubulin polymerization inhibitors targeting colchicine binding site. *Bioorg Chem* 2021;112:104965.